Available online at www.sciencedirect.com
ScienceDirect
Icarus 188 (2007) 481–505
ICARUS
www.elsevier.com/locate/icarus

Lifetimes of small bodies in planetocentric (or heliocentric) orbits

Anthony R. Dobrovolskis[a,*], José L. Alvarellos[b], Jack J. Lissauer[c]

[a] Lick Observatory, U.C. Santa Cruz, 245-3 NASA Ames Research Center, Moffett Field, CA 94035-1000, USA
[b] MS G-76, Space Systems Loral, 3825 Fabian Way, Palo Alto, CA 94303, USA
[c] Space Science and Astrobiology Division, 245-3 NASA Ames Research Center, Moffett Field, CA 94035-1000, USA

Received 31 July 2006; revised 18 November 2006
Available online 10 January 2007

Abstract

Stray bodies orbiting a planet or the Sun are removed by collisions with larger objects or by expulsion from the system. However, their rate of removal generally cannot be described by the simple exponential law used to describe radioactive decay, because their effective half-life lengthens with time. Previous studies of planetesimals, comets, asteroids, meteorites, and impact ejecta from planets or satellites have fit the number of survivors S vs elapsed time t using exponential, logarithmic, and power laws, but no entirely satisfactory functional form has been found yet. Herein we model the removal rates of impact ejecta from various moons of Jupiter, Saturn, and Neptune. We find that most situations are fit best by stretched exponential decay, of the form $S(t) = S(0)\exp(-[t/t_0]^{\beta})$. Here t_0 is the time when the initial population has declined by a factor of $e \approx 2.72$, while the dimensionless exponent β lies between 0 and 1 (often near 1/3). The e-folding time $S[\mathrm{d}S/\mathrm{d}t]^{-1}$ itself grows as the $[1-\beta]$ power of t. This behavior is suggestive of a diffusion-like process.

Keywords: Celestial mechanics

1. Introduction

The planets and their satellites grew from the accumulation of small solid bodies; the cratering records of the Moon and of other ancient surfaces bear witness to the presence of many stray bodies early in geologic history, declining with a half-life which has lengthened over time (e.g., Hartmann, 1972). Even today, the Solar System still is littered with small objects left over from the formation epoch, or created by more recent collisions. These stray bodies are removed by ejection from planetocentric or heliocentric orbit, as well as by colliding with planets, moons, and the Sun, with characteristic lifetimes depending on their orbits. (Other loss processes occur, such as cometary outgassing, tidal disruption, and collisions with other small debris, but these will not be considered herein.) However, as some orbits are much more stable than others, the rate at which a given population declines generally cannot be described by the simple exponential law used to describe radioactive decay.

In this paper we model the loss rates of stray particles, the better to understand the mechanisms by which small bodies are removed from various niches within the Solar System. We begin in Section 2 by using the removal of ejecta from Saturn's moon Hyperion to compare various proposed decay laws. Section 3 applies the techniques developed in Section 2 to Hyperion ejecta in greater depth, as well as to ejecta from other satellites of Saturn, Jupiter, and Neptune. Section 4 discusses the lessons learned from this study, while Section 5 reviews our conclusions. Finally, two appendices describe the fitting procedures and lifetime distributions.

2. Decay curves

Saturn's small satellite Hyperion is locked in a 4:3 mean motion resonance with the nearby much more massive moon Titan. We have used the "regularized" routine RMVS3 of the SWiFT mixed-variable symplectic integrator package (Levison and Duncan, 1994), based on techniques introduced by Wisdom and Holman (1991), to show that gravitational perturbations (mostly from Titan) can scatter ejecta from Hyperion throughout the saturnian system (Dobrovolskis and Lissauer, 2004). In

* Corresponding author. Fax: +1 (650) 604 6779.
E-mail address: dobro@cosmic.arc.nasa.gov (A.R. Dobrovolskis).

0019-1035/$ – see front matter © 2007 Elsevier Inc. All rights reserved.
doi:10.1016/j.icarus.2006.11.024

brief, each of our Hyperion simulations included Saturn and its moons Tethys, Dione, Titan, Hyperion, and Iapetus, as well as the Sun. For each integration, we ejected 210 massless particles vertically upward from points distributed roughly uniformly over Hyperion's surface. We then followed the evolution of this population as debris was removed by collisions with Saturn, its rings, or its above-mentioned moons, or by expulsion from orbit around Saturn. Non-gravitational forces were not considered. We shall use the results of these simulations to compare various functional forms proposed for the decay of the ejecta population.

Let T be the total number of test particles in the simulation, $S(t)$ the number of particles surviving at time t, and $R(t)$ the number removed by that time. Thus $R(0) = 0$, $S(0) = T$, and $R(t) + S(t) = T$ for any time t. Because the evolution of the population depends on its current members, it is convenient to treat the fraction $S(t)/T$ of particles surviving rather than the cumulative fraction removed $R(t)/T$. The lowermost curve (black) in Fig. 1 displays S/T versus t for the fiducial simulation of Dobrovolskis and Lissauer (2004), referring to the linear scales at the left-side and bottom axes, respectively. Because $R/T = 1 - S/T$, this curve is the same as the uppermost curve in Fig. 2 of Dobrovolskis and Lissauer (2004), but turned upside down. In this view it may be regarded as a "decay curve," describing the decline of the population of survivors with time.

Similar decay curves are characteristic of many orbit removal simulations (e.g., Gladman and Duncan, 1990; Holman and Wisdom, 1993; Levison and Duncan, 1994; Gladman et al., 1995, 1996, 2000, 2005; Dones et al., 1996, 1999a; Holman, 1997; Gladman, 1997; Farinella et al., 1997; Burns and Gladman, 1998; Malyshkin and Tremaine, 1999; Evans and Tabachnik, 1999; Tabachnik and Evans, 2000; Hartmann et al., 2000; Dobrovolskis et al., 2000; Robutel and Laskar, 2001; Armstrong et al., 2002; Chambers et al., 2002; Quintana et al., 2002; Alvarellos et al., 2002, 2005, 2007; Nesvorný and Dones, 2002; Nesvorný et al., 2003; Dobrovolskis and Lissauer, 2004; Zeehandelaar and Hamilton, 2005, 2006, 2007). Of the above, Gladman et al. (1995, Fig. 1a; 1996, Fig. 1; 2000, Fig. 2), Gladman (1997, Figs. 8 and 10); Farinella et al. (1997, Fig. 1), Burns and Gladman (1998, Fig. 2), and Robutel and Laskar (2001, Fig. 5) have plotted their results in a linear:linear format, and obtained shapes similar to the lowermost curve (black) in our Fig. 1.

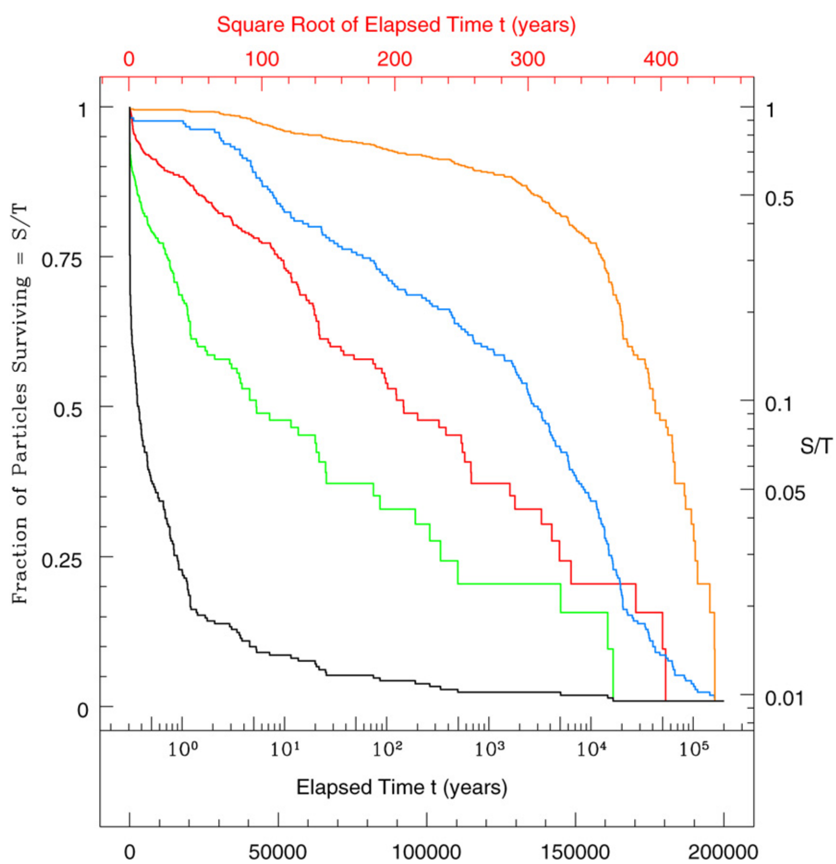

Fig. 1. Comparison of decay laws for ejecta from Hyperion. Note that these are not different fits to the same "data," but the results of a single simulation plotted in five different formats. All curves extend from the time of the first particle removal until the end of the simulation. Bottom curve (black): fraction S/T of particles surviving (left-hand scale) vs elapsed time t (bottom scale). This curve would be straight if decays were linear with time, as in Eq. (11). Top curve (gold): $\log(S/T)$ (right-hand scale) vs $\log t$ (interior scale). This curve would be straight for a simple power law decay, as in Eq. (1). Next-to-uppermost curve (blue): S/T (left-hand scale) vs $\log t$ (interior scale). This curve would be straight for a simple logarithmic decay, as in Eq. (2). Next-to-lowest curve (green): $\log(S/T)$ (right-hand scale) vs elapsed time t (bottom scale). This curve would be straight for a simple exponential decay, as in Eq. (5). Middle curve (red): $\log(S/T)$ (right-hand scale) vs $\sqrt{t}$ (top scale). This curve would be straight for a stretched exponential decay with $\beta = 1/2$, as in Eq. (9).

2.1. Power laws versus log laws

At first glance, the shape of the lowermost decay curve (black) in Fig. 1 suggests a functional form like $1/t$, or some other negative power of the time. In fact, this curve looks nearly self-similar when plotted over a wide range of linear time-scales, as a power law would. Accordingly, Evans and Tabachnik (1999, Eq. (1b)) (see also Tabachnik and Evans, 2000, Eq. (23)) have attempted to fit their results on removal of belts of remnant planetesimals between the terrestrial planets with the power law

$$S(t) = C/t^D \quad \Leftrightarrow \quad \log S = \log C - D \log t \tag{1a}$$

$$\Rightarrow \quad \mathrm{d}S/\mathrm{d}t = -CD/t^{D+1} = -SD/t, \tag{1b}$$

where C and D are dimensionless positive constants. Note that C is the number of survivors after one unit of time t has elapsed. Throughout this paper, we measure t in years, and we use "log" as standard notation for the base-10 or common logarithm ($\log_{10}$), and "ln" for the base-e or natural logarithm ($\log_e$).

Dones et al. (1996, 1999a), Holman (1997), and Hartmann et al. (2000) have employed similar power laws for removal of remnant planetesimals between the planets. Equation (1) would appear as a straight line of slope $-D$ and y-intercept $\log(C/T)$ on a graph of $\log(S/T)$ vs $\log t$. The uppermost curve (gold) in Fig. 1 plots our results in just this format, now referring to the right-side and interior axes, respectively. However, it is clear that this curve is not a straight line, so our decay behavior does not fit any simple power law. Levison and Duncan (1994, Figs. 5 and 11), Gladman et al. (1995, Fig. 1b), Holman (1997, Fig. 3), Dones et al. (1999a, Fig. 1), Quintana et al. (2002, Figs. 5 and 7), and Alvarellos et al. (2005, Fig. 6) have plotted their results in similar log:log formats, and obtained curves resembling ours.

Decay of orbiting populations has also been described as having a logarithmic form (Holman and Wisdom, 1993; Dones et al., 1999a, 1999b; Evans and Tabachnik, 1999, Eq. (1a); Tabachnik and Evans, 2000, Eq. (22); Hartmann et al., 2000, Eq. (4); Robutel and Laskar, 2001, Fig. 5). For example, Tabachnik and Evans (2000) have fitted their results also to the logarithmic decay law

$$S(t) = A - B \log t \tag{2a}$$

$$\Rightarrow \quad \mathrm{d}S/\mathrm{d}t = -B \log(e)/t \approx -0.4343B/t, \tag{2b}$$

where A and B are dimensionless positive constants too. Note that now A is the number of survivors after one time unit (year). One advantage of this formulation is that any linear combination of such "log laws" is a log law too; in this sense one might say that if you have seen one log law, you have seen them all. However, this superposition property is violated by the nonlinear stipulation that $S(t)$ must not go negative, but remains at zero once the population vanishes.

Equation (2) would appear as a straight line of slope $-B/T$ and y-intercept A/T on a graph of S/T vs $\log t$. The next-to-uppermost curve (blue) in Fig. 1 plots our results in this format, now referring to the left-side and interior axes, respectively. The resulting curve consists of roughly uniform steps, and is straighter than the lowest or uppermost curves, but still is not fitted well by any straight line. Similar linear:log formats were used by Gladman and Duncan (1990, Fig. 5), Holman and Wisdom (1993, Fig. 7), Tabachnik and Evans (2000, Figs. 20 and 21), Hartmann et al. (2000, Fig. 5b), Armstrong et al. (2002, Fig. 1), Chambers et al. (2002, Fig. 7), Alvarellos et al. (2002, Figs. 4, 7, and 10), Nesvorný and Dones (2002, Fig. 10), and Nesvorný et al. (2003, Fig. 5), who all obtained curves resembling ours.

In order to compare these decay laws, for each of our long-term simulations we performed linear least-squares fits of $S(t)$ to both functional forms (1) and (2), using the method described in Appendix A. Table 1 lists the resulting best fit parameters, along with their corresponding 1-sigma uncertainties (see Appendix A). For comparison with our fiducial case ($GM = 1.00\ \mathrm{km}^3/\mathrm{s}^2$), Table 1 also includes long-term (200,000-year) integrations for a massless Hyperion as well as for a massive proto-Hyperion (the cases in Table 3 of Dobrovolskis and Lissauer, 2004). In contrast, recent results from Cassini flybys reveal $GM \approx 0.389\ \mathrm{km}^3/\mathrm{s}^2$, so that Hyperion's density is only $\sim 476\ \mathrm{kg/m}^3$ (Luke Dones, 2006, personal communication).

Table 1 shows that C and A (the number of survivors after one year) are several percent less than T (the initial number of particles). This table also lists values of χ, a measure of the goodness of fit (see Appendix A). In general, the better the fit, the lower χ should be. Although the large values of χ for both laws indicate that neither fit is really satisfactory, they suggest that the logarithmic law (2) fits the decay slightly better than the power law (1), consistent with the impression from Fig. 1. Evans and Tabachnik (1999) also stated that the logarithmic law provided a better fit to their results than the power law, but they did not describe their fitting procedure.

Dones et al. (1996) found that their populations of remnant planetesimals decayed roughly exponentially at early times, but at late times they decayed as power laws with exponents ranging from 1.0 down to 0.3. Likewise Holman (1997) fitted the tail of his planetesimal decay curve to a power law with exponent 1.01 ± 0.13, consistent with unity, while Tabachnik and Evans (2000) reported values of the exponent D ranging from 1.60 down to 0.19 for trojan companions of the terrestrial planets. In contrast, Evans and Tabachnik (1999) obtained values of D ranging from 0.189 down to 0.040 for their planetesimal belts. Similarly, we find D ranging from 0.091 down to 0.060 for our ejecta, as listed in Table 1.

Such low exponents make the power law (1) difficult to distinguish from the logarithmic law (2). In fact, the logarithmic law can be seen as a limiting case of the power law as the power D tends to zero (provided that CD in Eq. (1b) simultaneously approaches $B \log e$ in Eq. (2b); indeed, these are approximately equal in Table 1). To see this, note that the time interval $t_1 \equiv |\mathrm{d}S/\mathrm{d}t|^{-1}$ between successive particle removals is directly proportional to the elapsed time t for the logarithmic law (2b), but proportional to t^{D+1} for the power law (1b). (The latter relation is known to seismologists as Omori's law when used with $D + 1 > 0$ to describe the frequency of earthquake aftershocks; Lay and Wallace, 1995, p. 385.)

Table 1
Fit parameters of various decay laws for different masses and radii of Hyperion

	GM of Hyperion	1.00 km^3/s^2	2.88 km^3/s^2	0
	Radius of Hyperion	143.0 km	190.0 km	143.0 km
	Initial particles T	210	210	210
Decay law	Final particles	2 (1%)	2 (1%)	34 (16%)
Simple power law (1)	D	0.0760 ± 0.0030	0.0908 ± 0.0032	0.0596 ± 0.0028
	C/T	0.961 ± 0.006	0.951 ± 0.004	0.958 ± 0.006
	χ	3.459	4.224	2.027
	t_0 (yr)	0.595	0.572	0.488
Shifted power law (3)	D	0.0921 ± 0.0036	0.1188 ± 0.0043	0.0672 ± 0.0033
	T_*/T	1.074 ± 0.009	1.105 ± 0.008	1.045 ± 0.009
	χ	3.153	3.758	1.780
Simple logarithmic law (2)	B/T	0.180 ± 0.003	0.189 ± 0.003	0.114 ± 0.003
	A/T	0.977 ± 0.007	0.957 ± 0.009	0.961 ± 0.006
	t_{00} (yr)	2.8×10^5	1.2×10^5	2.6×10^8
	χ	3.350	3.180	1.700
	t_0 (yr)	0.749	0.590	0.458
Shifted logarithmic law (4)	B/T	0.195 ± 0.003	0.201 ± 0.004	0.123 ± 0.004
	T_*/T	1.068 ± 0.010	1.058 ± 0.015	1.030 ± 0.008
	t_{00} (yr)	1.0×10^5	5.6×10^4	6.3×10^7
	χ	2.564	2.741	1.486
Simple exponential decay (5)	t_0 (yr)	$40{,}600 \pm 6743$	$42{,}269 \pm 15{,}664$	$161{,}126 \pm 20{,}324$
	T_*/T	0.430 ± 0.051	0.215 ± 0.065	0.564 ± 0.031
	χ	1.509	2.050	0.718
Stretched exponential decay (6)	t_0 (yr)	$4731 \times/\div 1.95$	$1411 \times/\div 1.99$	$51{,}659 \times/\div 2.90$
	β	0.328 ± 0.019	0.368 ± 0.025	0.229 ± 0.018
	χ	1.603	1.173	1.332
	t_E (yr)	8132	1250	58,160

Note. The simulation interval was 200,000 years in each case.

2.2. Time shifts

Note also that both Eqs. (1) and (2) lead to infinite values of S and dS/dt at $t = 0$. The singularity in dS/dt is benign, but that in S itself is more troublesome. In order to remove both of these singularities, we may shift the origin of time by some characteristic parameter $t_0 > 0$. Then Eq. (1) is amended to the "shifted power law"

$$S(t) = \frac{T}{[1 + t/t_0]^D} = \frac{T t_0^D}{[t_0 + t]^D} \tag{3a}$$

$$\Rightarrow \quad dS/dt = \frac{-T t_0^D D}{[t_0 + t]^{D+1}} = \frac{-SD}{t_0 + t}. \tag{3b}$$

Here the exponent D retains the same meaning it has in Eq. (1), while the parameter C has been supplanted by the constant $T = S(0)$, the total number of particles in the simulation. Certain natural phenomena, such as unforced turbulence (Frisch, 1995) and many chemical reactions (e.g., $X + X \to X_2$), decay as a power of the shifted time, as in Eq. (3).

Similarly, Eq. (2) becomes the "shifted log law"

$$S(t) = T - B\log(1 + t/t_0) = T + B\log t_0 - B\log(t_0 + t) \tag{4a}$$

$$\Rightarrow \quad dS/dt = \frac{-B\log e}{t_0 + t} \approx \frac{-0.4343B}{t_0 + t}, \tag{4b}$$

where the coefficient B retains the same meaning it has in Eq. (2), but the parameter A also has been displaced by T.

In both Eqs. (3) and (4), $S = T$ when $t = 0$, as required. In the opposite extreme, when $t \gg t_0$, Eqs. (3) and (4) reduce to Eqs. (1) and (2), respectively, where we identify $T = C/t_0^D$ and $T = A - B\log t_0$. Note that now the time interval $t_1 \equiv |dS/dt|^{-1}$ between successive particle removals is proportional to the shifted time $t_0 + t$ for Eq. (4), and to $[t_0 + t]^{D+1}$ for Eq. (3). The shifted logarithmic law (4) is a limiting case of the shifted power law (3) as the dimensionless exponent D again tends to zero (provided that now TD in Eq. (3b) simultaneously approaches $B\log e$ in Eq. (4b); in fact, these are approximately equal from Table 1).

We fitted our results for $S(t)$ to both time-shifted decay laws as well. These are still two-parameter fits, for the sake of a fair comparison with the other decay laws. In principle, we could specify the total number of particles T a priori and then solve for the parameters D and t_0 in Eq. (3), or for B and t_0 in Eq. (4). But instead, we found it more convenient to use the values of A, B, C, and D from the fits to Eqs. (1) and (2) to fix $t_0 = [C/T]^{1/D}$ in Eq. (3) and $t_0 = 10^{[A/B - T/B]}$ in Eq. (4) from the late-time limits above. We then solved for the best-fit initial number T_* of particles along with the slope parameters D and B/T in Eqs. (3) and (4). The results are listed in Table 1, along with the corresponding time shifts t_0; note that t_0 is output from the unshifted laws (1) and (2), but input to the shifted versions (3) and (4).

Note also that the time shifts t_0 are consistently only a fraction of a year, but much longer than Hyperion's orbital period of 21.3 days ≈ 0.0583 yr. The estimates of T_* are fairly realistic, but consistently several percent greater than their true value of $T = 210$. Comparison of the tabulated results shows that D and B/T are also slightly larger in magnitude for Eqs. (3) and (4) than for Eqs. (1) and (2); however, the fitness measure χ is smaller, so that the shifted decay laws do fit our simulations better than the unshifted decay laws. From these values of χ, Eq. (4) seems to be a better decay model than Eq. (3), but still neither fit is very close.

Although time shifts can improve the fit of the decay laws at early times, they cannot alleviate certain problems with decay at late times. Note that power-law decay (whether time-shifted or not) is never complete, since formally some particles always remain for either Eq. (1) or Eq. (3). In contrast, S vanishes at a finite time $t_{00} = 10^{A/B}$ for Eq. (2), or at $t_{00} = t_0[10^{T/B} - 1]$ for Eq. (4). Table 1 includes this "extinction time" t_{00} for both logarithmic laws; note that t_{00} is shorter for the shifted log law (4) than for its unshifted version (2). In fact, t_{00} is shorter than the simulation interval in three of the six cases.

The removal of all particles in a finite time is unphysical in principle. Furthermore, both logarithmic laws (2) and (4) generally fail to fit the first and last few percent of the removals; this is one reason why we ran most of our simulations to >99% completion (only <1% of the total particles surviving the run). Along with the need for a better fit, these behaviors lead us to seek a more realistic decay law.

2.3. Simple exponential decay

Like the power laws, exponential decay is never formally complete. Classic exponential decay is described by

$$S(t) = T\exp(-t/t_0) \quad \Leftrightarrow \quad \log S = \log T - t\log(e)/t_0$$
$$\Rightarrow \quad \mathrm{d}S/\mathrm{d}t = -\frac{T}{t_0}\exp(-t/t_0) = -S/t_0, \tag{5}$$

where $t_0 > 0$ is again a time constant. For Eq. (5), the time interval $t_1 \equiv |\mathrm{d}S/\mathrm{d}t|^{-1}$ between successive particle removals grows exponentially with time, but a fixed fraction of the remainder are removed during each unit of time. This familiar law governs simple radioactive decay, for example, where half of a given radionuclide decays during each "half-life" $t_{1/2} = t_0 \ln 2 \approx 0.6931 t_0$. The e-folding time $t_e \equiv S|\mathrm{d}S/\mathrm{d}t|^{-1} = St_1$ is simply the constant t_0. For comparison, the e-folding time grows linearly with time for the shifted power law (3): $t_e = [t_0 + t]/D$.

Note that the logarithm of S declines linearly with time for Eq. (5); this would appear as a straight line of slope $-\log(e)/t_0 \approx -0.4343/t_0$ and y-intercept zero on a plot of $\log(S/T)$ versus t. The next-to-lowest curve (green) in Fig. 1 plots our results in this format, now referring to the right-side and bottom axes, respectively. The resulting curve again is straighter than the uppermost or lowest curves (apart from the steps due to small-number statistics), but still is not fit well by any single straight line. Dones et al. (1996, Fig. 2), Hartmann et al. (2000, Fig. 5a), Gladman et al. (2005, Fig. 4), and Zeehandelaar and Hamilton (2005, 2006) plotted their results in the same log:linear format, and obtained shapes similar to the green curve in our Fig. 1.

As we did for the logarithmic and power laws (1)–(4), we fitted our results for $S(t)$ to the simple exponential law (5). Because Eq. (5) depends on only one parameter t_0, we again solved for the best-fit initial number T_* of particles as well, as with the shifted laws (3) and (4), for the sake of a fairer comparison with the other two-parameter fits. But as shown in Table 1, now the estimates of T_* are considerably less than its true value $T = 210$, because our decays do not really follow a simple exponential law. Nevertheless, these fits give fairly low values of χ (ranging from 0.718 to 2.050) compared to the previous decay laws.

2.4. Stretched exponential decay

A useful generalization of Eq. (5) is the Kohlrausch formula

$$S(t) = T\exp\bigl(-[t/t_0]^\beta\bigr)$$
$$\Rightarrow \quad \mathrm{d}S/\mathrm{d}t = \frac{-\beta T}{t^{1-\beta}t_0^\beta}\exp\bigl(-[t/t_0]^\beta\bigr) = \frac{-\beta S}{t^{1-\beta}t_0^\beta}. \tag{6}$$

Here the logarithm of S/T decays as a power $\beta > 0$ of the time. For $\beta = 1$, Eq. (6) reduces to the simple exponential law Eq. (5). Otherwise Eq. (6) becomes a power law, resembling a parabola, in the log:linear format of the green curve in Fig. 1. As in the power laws (1) and (3), some particles nominally survive to arbitrarily long times.

For $0 < \beta < 1$, $\mathrm{d}S/\mathrm{d}t$ is formally infinite at $t = 0$, but $S(t)$ itself always remains finite, while the e-folding time

$$t_e \equiv S|\mathrm{d}S/\mathrm{d}t|^{-1} = St_1 = t^{1-\beta}t_0^\beta/\beta \tag{7}$$

itself lengthens as the $[1-\beta]$ power of the time. This case is known to solid-state physicists as "stretched exponential relaxation," while β is known as the stretching parameter; it has been used to describe various physical phenomena, including creep, annealing, electrical impedance, and magnetic spin relaxation (e.g., Palmer et al., 1984; Peterson, 1989; Halsey and Leibig, 1991; Scher et al., 1991; Wikipedia, 2007). Stretched exponential decay is associated with the concept of "fractal time" because relaxation occurs on all time-scales (Peterson, 1989).

For $\beta > 1$, in contrast, t_e shortens with the passage of time; such behavior could be termed "compressed exponential relaxation." For all of our previous decay laws (1)–(5), the decay curve $S(t)$ is concave upward at all times, so that the absolute decay rate $|\mathrm{d}S/\mathrm{d}t|$ is greatest at the outset $t = 0$. In compressed exponential decay, in contrast, $\mathrm{d}S/\mathrm{d}t$ vanishes at $t = 0$, while $S(t)$ is concave downward for early times $t < t_0[1 - 1/\beta]^{1/\beta}$, but is concave upward thereafter. For example, if $\beta = 2$ this inflection point occurs at $t = t_0\sqrt{1/2} \approx 0.7071 t_0$, and function (6) is equivalent to the right half of a Gaussian distribution. In the extreme case $\beta = \infty$, $S(t)$ is a step function; all particles survive until $t = t_0$, and then suddenly expire.

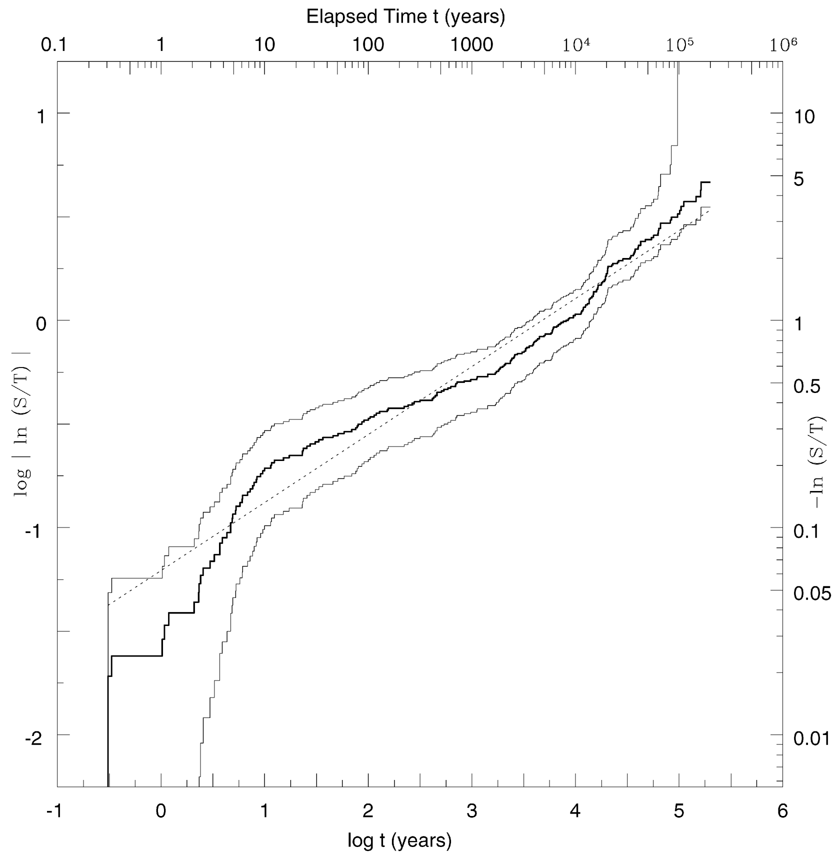

Fig. 2. Stretched exponential decay of ejecta from Hyperion. The heavy middle curve graphs $\ln(S/T)$ versus elapsed time, in a log:log format. The upper and lower curves display its three-sigma error envelope, while the dotted line represents a least-squares fit with slope 0.328; this slope is the exponent β in Eq. (6). For comparison, the diagonals of this plot (not drawn) have slopes of $\pm 1/2$.

In order to fit our results to the Kohlrausch law (6), we took the logarithm of both sides, twice:

$$\ln(S/T) = -[t/t_0]^\beta$$
$$\Leftrightarrow \quad \log\left|\ln(S/T)\right| = \log\left([t/t_0]^\beta\right) = \beta \log t - \beta \log t_0. \qquad (8)$$

Fig. 2 graphs $\log|\ln(S/T)|$ versus $\log t$ for our fiducial decay curve, along with its three-sigma uncertainty envelope (see Appendix A) and the best-fitting regression line. In this format, Eq. (6) plots as a straight line of slope β and intercept $-\beta \log t_0$.

Our best estimates for these parameters are also listed in Table 1, along with the fitness measure χ, ranging from 1.173 to 1.603. The latter are comparable to χ for the simple exponential model (5); however, this is because the simple exponential fits included the second parameter T_*. If the simple exponential, shifted logarithmic, or shifted power law fits had been constrained to have $T_* = T$, all three values of χ would have been larger than tabulated.

The final line of the table gives t_E, the time at which the number S of surviving particles falls to $1/e \approx 0.3679$ of the initial number T. In principle, this should equal t_0 for simple exponential decay (5) or for stretched exponential decay (6). In fact $t_E \ll t_0$ for the simple exponential fits, but $t_E \approx t_0$ for the stretched exponential fits. This provides further evidence that the stretched exponential model is actually more realistic than the simple exponential model.

Although t_0 for the stretched exponential fits is uncertain by a factor of two or three, it varies more than this from case to case: while $t_0 \approx 5000$ yr in our fiducial case, it is only $\sim$1000 yr for the larger, massive Hyperion but $\sim$50,000 yr for the massless Hyperion. Evidently Hyperion's own gravity is important for scattering its ejecta into harm's way, as discussed by Dobrovolskis and Lissauer (2004).

In contrast to t_0, β varies rather little; its best-fitting values in Table 1 are all around 0.3, so that the e-folding time t_e grows roughly as the $[1-\beta] \approx 0.7$ power of the time t. It is tempting to suppose that orbit removals are controlled by some kind of diffusion process such that t_e grows as the square root of the time, so β is actually 1/2.

If indeed $\beta = 1/2$, the Kohlrausch law (6) becomes

$$S(t) = T \exp(-\sqrt{t/t_0}) \quad \Leftrightarrow \quad \ln(S/T) = -\sqrt{t/t_0}$$
$$\Rightarrow \quad \mathrm{d}S/\mathrm{d}t = \frac{-T/2}{\sqrt{t_0 t}} \exp(-\sqrt{t/t_0}) = \frac{-S/2}{\sqrt{t_0 t}}. \qquad (9)$$

Equation (9) would appear as a straight line of slope $-0.4343/\sqrt{t_0}$ and zero intercept on a graph of $\log(S/T)$ vs $\sqrt{t}$. Accordingly, the middle curve (red) in Fig. 1 plots our fiducial results in just this format. In this log:root format, our decay curve finally becomes nearly a straight line!

2.5. Diffusion

As stated above, the stretched exponential law suggests a process of diffusion in the space of orbital elements. However, diffusion in semi-major axis actually bears more resemblance to *compressed* exponential decay; at least for the escape of comets from the Oort cloud by diffusion in orbital binding energy, according to Yabushita's (1980) analytical solution as well as to the random walk model of Dones et al. (1996), although both of those studies employed idealized initial conditions in which particle trajectories began far from harm's way. Yabushita's (1980) solution is given as an incomplete gamma function (see also Dones et al., 1996); we find that this function can also be written in elementary form as

$$f(t) \equiv S(t)/T = \gamma(2, z) \equiv \int_0^z e^{-u} u \, du = 1 - [1 + z]e^{-z}$$

$$\Rightarrow \quad df/dt = \frac{df}{dz}\frac{dz}{dt} = -z^3 e^{-z}/\bar{t}, \tag{10}$$

where u is a dummy variable, and $z \equiv 8t_d/t = \bar{t}/t$. Here t_d is the "diffusion time" of the comet cloud, and $\bar{t} = 8t_d$ is the mean lifetime of the particles, as explained in Appendix B.

Solution (10) is graphed in Fig. 3, in five formats similar to those of Fig. 1. As in compressed exponential decay, df/dt from Eq. (10) vanishes at $t = 0$. Likewise $f(t)$ also is concave downward for $t < \bar{t}/3 = 8t_d/3 \approx 2.6667t_d$ ($z > 3$, $f \gtrsim 0.8009$), and is concave upward thereafter. Because the decay curves $S(t)$ of our simulations are essentially concave upward at all times, we did not attempt to fit them to the diffusion solution (10). However, we will reconsider diffusion phenomena in Section 4.

For $t \gg \bar{t} = 8t_d$ ($z \ll 1$), Eq. (10) approaches $f(t) = z^2/2 = \bar{t}^2/2t^2 = 32t_d^2/t^2$. Thus the population decays steeply as the inverse square of the time for late times, as shown by the log:log plot (golden curve) in Fig. 3. The random walk simulations of Dones et al. (1996) showed a similar inverse-square law tail. Note that this asymptotic behavior is equivalent to the simple power law (1) for $D = 2$ and $C/T = \bar{t}^2/2 = 32t_d^2$, or to the shifted power law (3) for $D = 2$ and $t_0^2 = \bar{t}^2/2 = 32t_d^2$. However, this value for the exponent D is greater than any considered heretofore. In contrast, both the numerical integrations of Dones et al. (1996) and the Keplerian mapping technique of Malyshkin and Tremaine (1999) found that the population of simulated comets declines almost as a simple exponential decay at first, but eventually as a slower power law with exponent D closer to 1 than to 2.

3. Case studies

3.1. More Hyperion

The format of Figs. 1 and 3 is convenient for discussing the decay curves of other test populations, as well. For example,

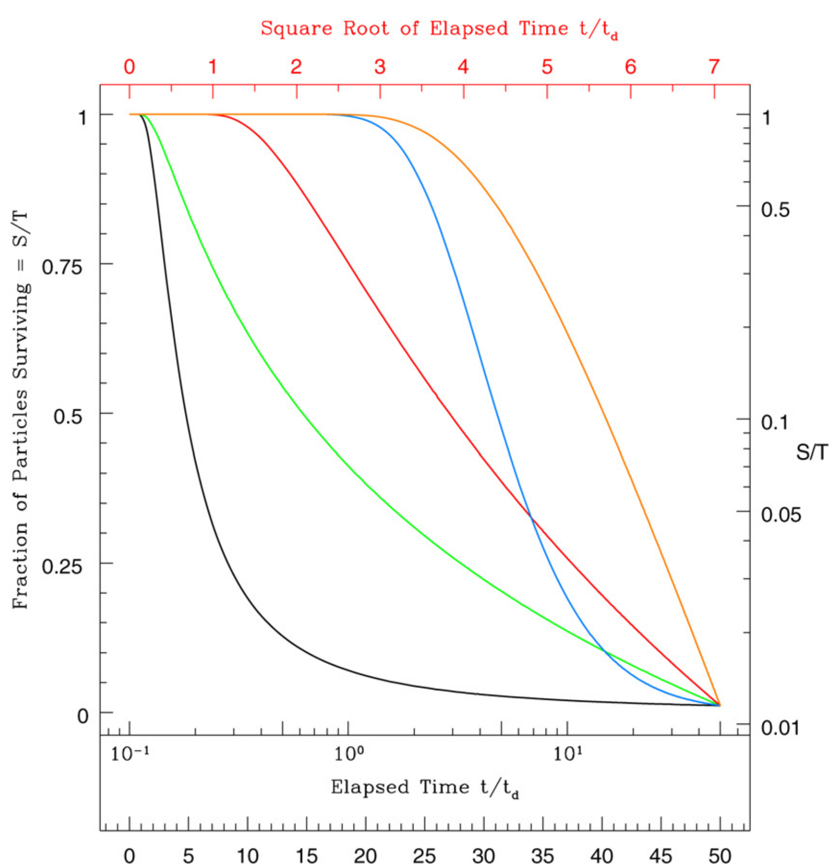

Fig. 3. Diffusion solution, Eq. (10). Format similar to Fig. 1.

Table 2
Fit parameters of various decay laws for different launch speeds from Hyperion

	Launch speed	$1.01V_e$	$1.05V_e$	$1.10V_e$	$2.00V_e$	$5.00V_e$	No Sun
	Initial particles T	208	210	210	210	210	210
Decay law	Final particles	44 (21%)	38 (18%)	39 (19%)	40 (19%)	82 (39%)	21 (10%)
Simple	D	0.0236	0.0636	0.0690	0.0535	0.0273	0.0650
power	C/T	1.016	1.016	0.959	0.937	0.984	0.954
law (1)	χ	4.275	2.628	2.218	3.579	4.127	3.039
	t_0 (yr)	1.918	1.269	0.548	0.298	0.495	0.487
Shifted	D	0.0346	0.0768	0.0824	0.0738	0.0432	0.0779
power	T_*/T	1.034	1.056	1.061	1.068	1.047	1.060
law (3)	χ	4.181	2.343	1.728	2.582	3.425	2.843
Simple	B/T	0.0812	0.140	0.136	0.124	0.0750	0.154
logarithmic	A/T	1.031	1.016	0.963	0.937	0.983	0.966
law (2)	t_{00} (yr)	4.9×10^{12}	1.9×10^7	1.2×10^7	3.5×10^7	1.3×10^{13}	1.9×10^6
	χ	5.672	2.662	1.810	3.201	4.220	3.255
	t_0 (yr)	2.387	1.308	0.532	0.313	0.590	0.603
Shifted	B/T	0.116	0.160	0.151	0.149	0.106	0.175
logarithmic	T_*/T	1.054	1.050	1.042	1.056	1.046	1.060
law (4)	t_{00} (yr)	1.0×10^9	2.3×10^6	2.2×10^6	1.6×10^6	1.5×10^9	3.0×10^5
	χ	5.161	2.295	1.353	1.939	3.041	2.809
Simple	t_0 (yr)	11,863	12,715	16,741	15,515	29,974	9270
exponential	T_*/T	0.872	0.723	0.626	0.597	0.700	0.645
decay (5)	χ	1.777	0.972	0.827	1.102	1.624	1.135
Stretched	t_0 (yr)	9506	8503	7447	5015	14,739	3733
exponential	β	0.618	0.348	0.287	0.321	0.380	0.356
decay (6)	χ	0.864	1.402	1.389	1.384	1.530	1.172
	t_E (yr)	8083	7565	8132	6916	>20,000	4077

Note. The simulation interval was only 20,000 years in each case.

the other cases listed in Table 1 produce plots similar to Fig. 1 (although the vertical range differs for the massless Hyperion case). In each case, the stretched exponential model fits best (produces the straightest decay curve).

Dobrovolskis and Lissauer (2004) also performed short-term (20,000-year) simulations to test the effects of the speed of ejection from Hyperion, as listed in their Table 4. Table 2 of this paper lists the results of fitting those runs to decay laws (1)–(6); the format is similar to our Table 1, but without the error bars. The top line of Table 2 gives the speed of ejection in terms of Hyperion's escape velocity V_e. The column headed "$1.10V_e$" is the same case as our fiducial run, but restricted to the first 20,000 years; note how decay is already 81% complete, compared to 99% for the full 200,000-year term. The column headed "No Sun" is another 20,000-year test with launch speed $1.10V_e$, but excluding the Sun as a perturber for comparison. Presumably solar perturbations raise the periapses of far-flung ejecta, and thereby lengthen their lifetimes.

The second line of the column headed "$1.01V_e$" lists only 208 initial particles instead of 210, because we ignored two ejecta which returned to Hyperion's surface within 7 days. For such low ejection speeds (in this case only one percent faster than the nominal escape velocity), a few particles follow short sub-orbital (ballistic) trajectories like these, or else they become temporary satellites (sub-satellites) of their source moon with lifetimes comparable to its orbital period; in either case, they never get outside of that moon's Hill sphere (Alvarellos et al., 2002). In order to exclude them from consideration, following Alvarellos et al. (2005), we ignored any particles which were removed in less than two orbital periods of their source. This should not seriously compromise our analysis, because the time-scales listed in Tables 1 and 2 (and Table 3) are all much greater than Hyperion's orbital period of 21.3 days ≈ 0.0583 yr.

Because of the short integration times, the simulations reported in Table 2 are much less complete than those of Table 1. Nevertheless the values of D and B for the power and logarithmic models (both simple and shifted) are similar to those in Table 1. Also as in Table 1, the values of C and A again fall within several percent of T (the initial number of particles) for the simple power and log laws (1) and (2); likewise for their shifted versions (3) and (4), the estimates T_* of the initial number of particles remain several percent greater than its true value T. For the simple exponential model (5), the estimate T_* is again considerably less than its true value T.

As in Table 1, all time-scales in Table 2 remain much greater than Hyperion's orbital period. Once more we find that time shifts t_0 on the order of a year slightly improve the fits to the logarithmic and power laws, and slightly increase D and B. As in Table 1, the extinction time t_{00} is shorter for the shifted log law (4) than for its unshifted version (2), but t_{00} is greater than the simulation interval for all cases in Table 2, and much greater than the values in Table 1. Again we find that the fit-

Table 3
Fit parameters of various decay laws for seasonal Hyperion runs

Decay law	True anomaly at launch	0°.42	97°.29	179°.94	263°.11	280°.81	Combined
	Initial particles T	209	210	210	210	210	1049
	Final particles	5 (2%)	5 (2%)	10 (5%)	9 (4%)	8 (4%)	37 (3.5%)
Simple power law (1)	D	0.0661	0.0735	0.0577	0.0657	0.0749	0.0634
	C/T	0.977	0.951	0.970	0.948	0.961	0.946
	χ	4.467	3.417	3.945	3.618	3.259	8.484
	t_0 (yr)	0.704	0.503	0.590	0.443	0.588	0.417
Shifted power law (3)	D	0.0915	0.0897	0.0761	0.0798	0.0906	0.0808
	T_*/T	1.083	1.075	1.063	1.064	1.072	1.071
	χ	3.801	3.117	3.256	3.365	2.923	7.438
Simple logarithmic law (2)	B/T	0.183	0.179	0.154	0.163	0.170	0.164
	A/T	0.984	0.969	0.971	0.955	0.973	0.950
	t_{00} (yr)	2.4×10^5	2.5×10^5	2.0×10^6	7.0×10^5	5.3×10^5	6.4×10^5
	χ	4.348	3.537	4.408	3.793	3.192	8.951
	t_0 (yr)	0.815	0.675	0.646	0.532	0.698	0.494
Shifted logarithmic law (4)	B/T	0.205	0.198	0.175	0.182	0.188	0.184
	T_*/T	1.079	1.074	1.063	1.067	1.064	1.072
	t_{00} (yr)	6.2×10^4	7.5×10^4	3.4×10^5	1.7×10^5	1.5×10^5	1.4×10^5
	χ	2.775	2.713	3.268	3.112	2.535	6.646
Simple exponential decay (5)	t_0 (yr)	26,417	24,550	33,019	33,139	31,128	29,993
	T_*/T	0.420	0.485	0.545	0.464	0.490	0.475
	χ	1.869	1.379	1.472	2.056	1.476	3.610
Stretched exponential decay (6)	t_0 (yr)	3349	3974	7358	4891	5054	4755
	β	0.393	0.342	0.337	0.336	0.321	0.346
	χ	0.972	1.233	1.664	1.645	1.558	2.940
	t_E (yr)	4066	6019	9441	6575	8132	6616

Note. The simulation interval was 100,000 years in each case.

ness measure χ is comparable for the two-parameter simple and stretched exponential models, but that t_E matches t_0 better for the stretched exponential law (6) than for the simple exponential law (5). And as before, we find that the stretching parameter β mostly ranges around $1/3$.

In order to test the effects of Hyperion's orbital eccentricity, Dobrovolskis and Lissauer (2004) also performed intermediate-term (100,000-year) integrations, listed as "seasonal simulations" in their Table 5. Note that the final two columns of that table contain errors: the last two entries in the row entitled "Survived" should be 8 (4%) and 37 (3.5%), while those in the "Escaped" row should be 21 (10%) and 91 (8.7%), and those in the row "Hit Titan" should be 162 (77%) and 814 (78%).

Table 3 of this paper lists the results of fitting those seasonal runs to decay laws (1)–(6), in a format similar to our Tables 1 and 2. The top line of Table 3 gives Hyperion's orbital position as its true anomaly at the time of ejection. The column headed "0°.42" refers to launch near Hyperion's periapsis, while the one labeled "179°.94" refers to its apoapsis. The column headed "263°.11" is the same case as our fiducial run, but restricted to the first half of the simulation; note how decay is so well advanced that only a few percent of the ejecta remain. The column labeled "Combined" lists the results of fitting the combination of all five seasonal runs.

Generally the results in Table 3 are similar from column to column, systematically varying somewhat with the true anomaly at launch. Again we find values of all parameters consistent with Tables 1 and 2. Once more, the stretched exponential law (6) generally fits our results best, as evidenced by the low values of the fitness measure χ for this model, particularly for ejection at periapsis. The combined run also fits the stretched exponential model best, although for each decay model, χ is greatest for the combined run. This is partly due to actual differences among the decay curves degrading the fit; but for reasons we do not fully understand, χ also tends to increase roughly as the square root of T, the total number of particles (i.e., $\chi^2 \sim T$). Randomly sampling only 210 particles of the combined run gives similar results to the five original runs.

Fig. 4 shows the decay curves for the combined simulations, in a similar format to Figs. 1 and 3. Again the stretched exponential model (red curve) is straightest. Note how combining runs reduces the shot noise and improves the statistics. In our subsequent simulations, we employ at least a hundred initial particles, but over a thousand ejecta are preferable.

3.2. *Other satellites of Saturn*

Subsequent to the Hyperion simulations of Dobrovolskis and Lissauer (2004), Alvarellos et al. (2005) undertook a study of

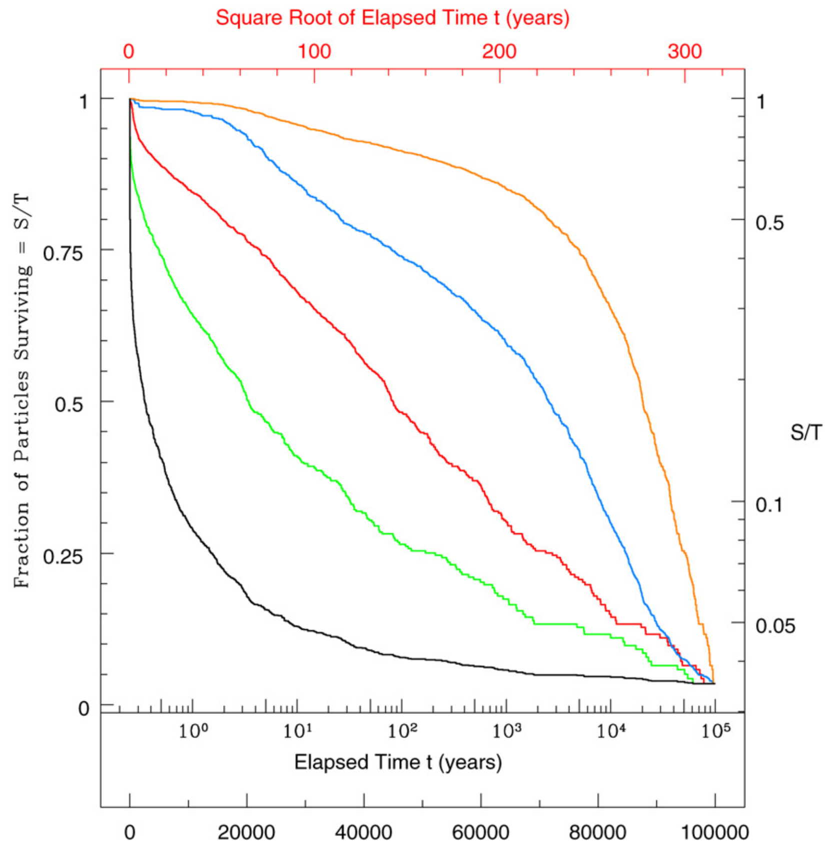

Fig. 4. Comparison of decay laws for combined seasonal Hyperion simulations (final column in Table 3). Format similar to Fig. 1.

ejecta from some of Saturn's other moons. They ejected 600 particles from each of the major craters Herschel on Mimas, Odysseus and Penelope on Tethys, and Tirawa on Rhea (although not all particles achieved planetocentric orbit; see Table 4). In an effort to be realistic, Alvarellos et al. (2005) used two end-member spray patterns, corresponding to rubble from loose regolith and to spalls from hard surfaces. In general, spall velocities were faster and more vertical, but the rubble and spall simulations do not differ greatly, as Table 4 indicates.

Table 4 displays the outcome of fitting the resulting decay curves to laws (1)–(6), in a format like Tables 1–3. Comparison shows that the time-scales vary from satellite to satellite, but that the dimensionless fit parameters remain similar. Note that β in Table 4 is about $1/2$, versus values nearer $1/3$ from Tables 1–3. The fitness measures χ in Table 4 are generally larger than those from Tables 1–3, but again the stretched exponential model (6) clearly fits best. Furthermore, t_E matches t_0 from the stretched exponential model (6) much better than t_0 from the simple exponential model (5).

To demonstrate, Figs. 5–7 respectively plot the decay curves for spalls from Herschel on Mimas, for rubble from Odysseus on Tethys, and for spalls from Tirawa on Rhea, in a format similar to Figs. 1, 3, and 4. Note how alike all of these curves are, although the time-scales differ considerably. In each case, the stretched exponential model (red curve) yields the best (straightest) fit. The results for ejecta from Penelope (not shown) are similar to those from Odysseus.

We believe that the stretching parameter β tends to be larger for these saturnian moons than for Hyperion or the satellites of Jupiter because the mid-sized satellites of Saturn are dynamically more isolated. From examination of the orbits, we find less spreading of the ejecta torus by perturbations from the other satellites. Hence the decay curve is less "stretched" than for Hyperion, or a dynamically crowded system like the Galilean satellites.

3.3. Moons of Jupiter

In an earlier series of simulations, Alvarellos et al. (2002) integrated ejecta from Jupiter's largest moon Ganymede, under the gravitational influences of Jupiter and its oblateness, all four Galilean satellites Io, Europa, Ganymede, and Callisto, as well as the Sun and Saturn. Particles were launched outward from the rim of Gilgamesh, the largest impact basin on Ganymede, at various speeds, and at angles of 30°, 45°, or 60° from the vertical, and were followed for 100,000 years, or until all particles were removed.

Alvarellos et al. (2002) tabulated their results according to the angle of ejection, but the outcomes actually depend more on the launch speed. Accordingly we have combined their simulations with the same launch speeds but different ejection angles. Table 5 displays the outcome of fitting the resulting decay curves to laws (1)–(6), in a format similar to Tables 1–4. Again, the dimensionless fit parameters are comparable to those from the previous tables, but the time-scales are different.

Table 4
Fit parameters of various decay laws for different moons of Saturn

	Satellite	Mimas		Tethys				Rhea	
	Orbital period	0.00258 yr		0.00517 yr				0.0124 yr	
	Run time	1000 yr		2000 yr				15,000 yr	
	Crater	Herschel		Odysseus		Penelope		Tirawa	
	Ejecta	Rubble	Spalls	Rubble	Spalls	Rubble	Spalls	Rubble	Spalls
	Initial particles T	526	554	555	595	561	590	582	600
Decay law	Final particles	2	3	7	5	3	4	2	4
Simple	D	0.0971	0.0348	0.103	0.0733	0.0612	0.107	0.0481	0.0526
power	C/T	0.831	0.874	0.782	0.825	0.830	0.714	0.892	0.898
law (1)	χ	6.348	8.298	7.451	8.651	9.481	7.649	9.163	8.733
	t_0 (yr)	0.149	0.0212	0.0908	0.0725	0.0474	0.0434	0.0937	0.130
Shifted	D	0.125	0.0552	0.142	0.110	0.106	0.151	0.0764	0.0767
power	T_*/T	1.092	1.050	1.112	1.091	1.092	1.123	1.064	1.062
law (3)	χ	6.051	7.699	6.507	7.575	8.198	6.358	8.155	7.901
Simple	B/T	0.262	0.213	0.239	0.232	0.227	0.226	0.199	0.202
logarithmic	A/T	0.791	0.707	0.755	0.743	0.707	0.692	0.803	0.829
law (2)	t_{00} (yr)	1041	2080	1457	1611	1322	1157	10,981	12,741
	χ	6.822	16.027	5.693	8.869	10.413	6.298	11.522	10.868
	t_0 (yr)	0.159	0.0422	0.0940	0.0781	0.0512	0.0435	0.102	0.141
Shifted	B/T	0.291	0.246	0.261	0.256	0.249	0.243	0.216	0.221
logarithmic	T_*/T	1.092	1.102	1.081	1.087	1.086	1.071	1.077	1.078
law (4)	t_{00} (yr)	438.7	485.9	634.7	627.5	527.1	560.9	4249	4786
	χ	5.365	11.600	4.205	6.109	7.408	5.671	8.217	7.827
Simple	t_0 (yr)	160.8	147.4	374.1	329.1	289.6	328.6	2036	2256
exponential	T_*/T	0.686	0.778	0.444	0.508	0.457	0.341	0.402	0.450
decay (5)	χ	3.012	2.737	4.385	4.622	4.612	4.182	4.084	4.176
Stretched	t_0 (yr)	64.44	74.73	48.61	55.39	32.82	24.61	216.8	323.7
exponential	β	0.535	0.620	0.479	0.521	0.512	0.442	0.490	0.495
decay (6)	χ	2.428	2.062	1.659	1.693	2.260	2.026	1.480	1.118
	t_E (yr)	79.09	86.87	45.99	56.68	28.78	23.98	196.6	327.1

As in Table 2, the top line of Table 5 lists the speed of ejection in terms of Ganymede's escape velocity V_e. The trend of these results with launch speed indicates that faster ejecta take longer to decay. This is especially clear from the final line of Table 5, and from t_0 for the stretched exponential law (6). Note also how the exponent β from the stretched exponential fit rises monotonically with launch speed from $\sim 1/4$ for the slowest ejecta to $\sim 1/2$ for the fastest ejecta.

Particles ejected with speeds slightly less than Ganymede's escape velocity $V_e \approx 2.740$ km/s still can escape, because they need only to reach Ganymede's Hill sphere rather than infinity (Alvarellos et al., 2002). However, the power and log law fits to ejecta with launch speeds $\leqslant V_e$ in Table 5 show values of the time shift t_0 only a few times greater than Ganymede's orbital period of 7.155 days ≈ 0.0196 yr. This suggests that t_0 may be overestimated; in fact, comparison of the fitness measures χ for the simple and shifted logarithmic laws (2) and (4) implies that including this time shift actually degrades the fit. The tabulated values of χ imply that the decays fit the stretched exponential law (6) better than the power and log laws (1)–(4) in every case.

The last column of Table 5, headed "Vertical," refers to a special test run in which 167 ejecta were launched vertically upward from the center of Gilgamesh, at speeds ranging uniformly from $0.903V_e$ to $1.400V_e$. However, the first 18 particles followed suborbital trajectories, while the next two entered temporary sub-satellite orbits around Ganymede; only the 147 vertical ejecta with launch speeds $\geqslant 0.963V_e$ escaped Ganymede and were fitted to the decay laws (1)–(6). Comparison with the other columns of Table 5 shows that on the average, these vertical ejecta behave most like the oblique ejecta with a launch speed of $1.20V_e$. However, note that the vertical ejecta fit a stretched exponential decay best of all, despite their wide range of launch speeds.

Recently Alvarellos et al. (2007) (see also Zahnle et al., 2007) also have simulated the evolution of rubble and spalls ejected from Io (period ≈ 1.769 days ≈ 0.00484 yr) by cometary impacts at four different locations: Io's south pole, its sub-jovian and anti-jovian points, and Io's apex of motion (at the center of its leading hemisphere). Table 6 lists the results of fitting all four decay curves to laws (1)–(6) for the spalls, while Table 7 does the same for the rubble. The results from all four impact sites were so similar that we have combined them into two large simulations, whose fit parameters are reported in Tables 6 and 7 as well. The tabulated values of χ imply that the stretched exponential law (6) again fits best in all ten cases. The composite decay curve for all of the spalls is plotted in the usual

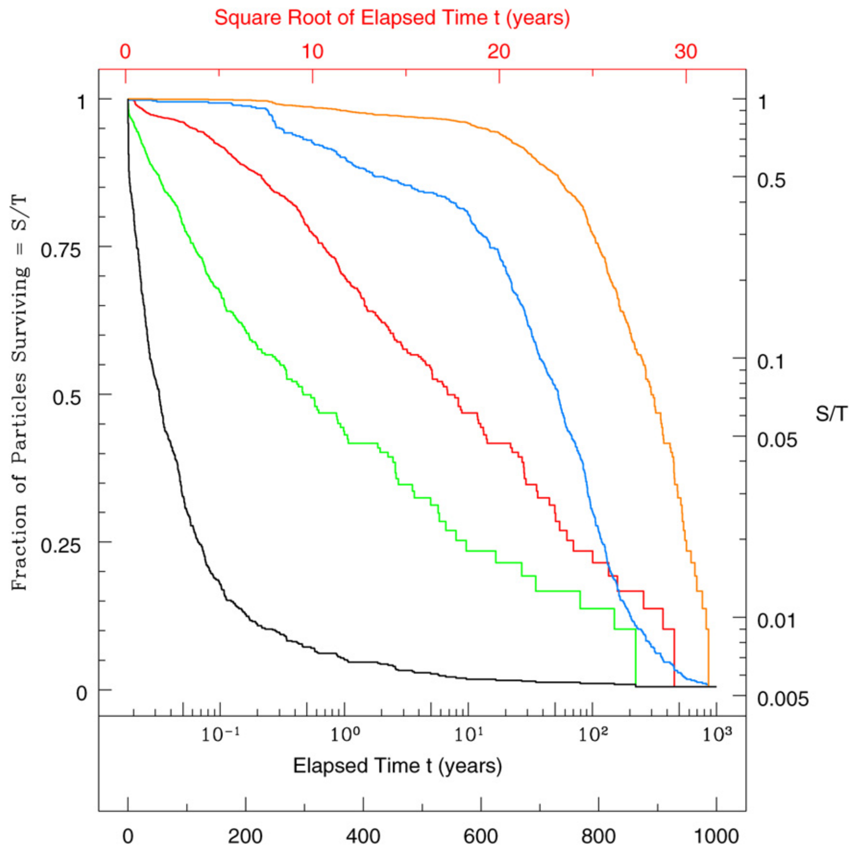

Fig. 5. Comparison of decay laws for spalls from Mimas. Format similar to Fig. 1.

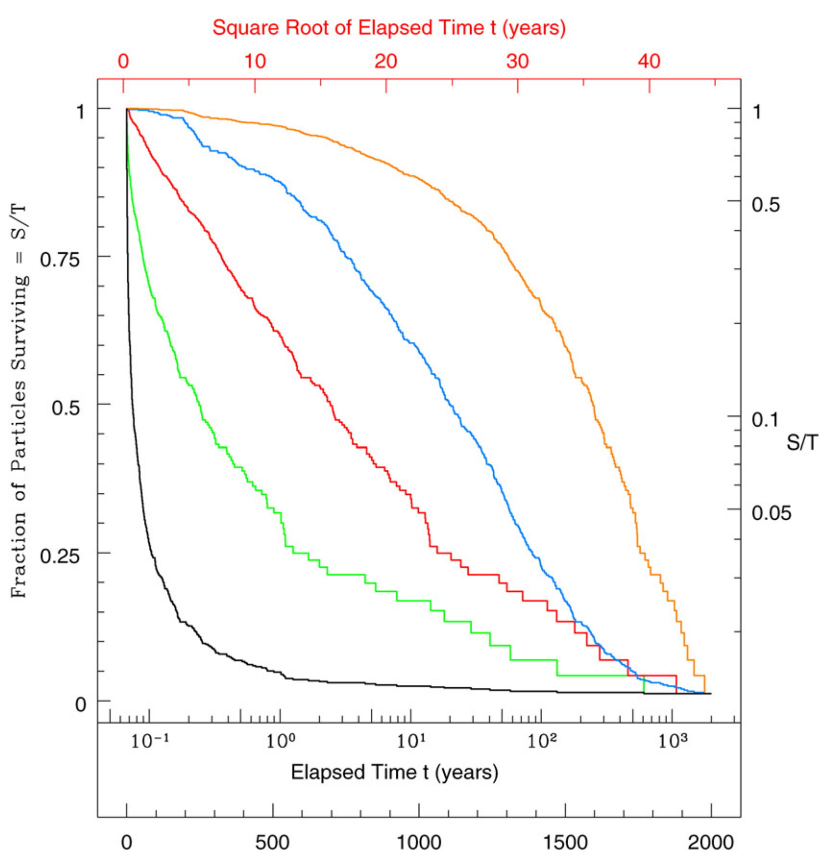

Fig. 6. Comparison of decay laws for rubble from Odysseus, on Tethys. Format similar to Fig. 1.

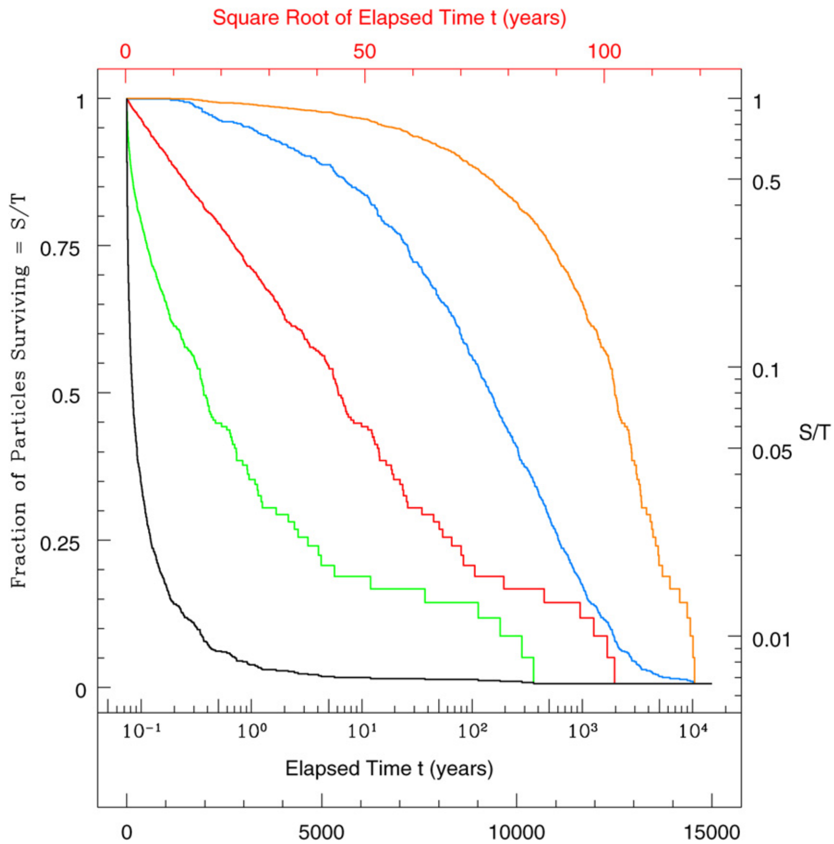

Fig. 7. Comparison of decay laws for spalls from Rhea. Format similar to Fig. 1.

formats in Fig. 8; that for the rubble is similar, but with shorter time-scales, consistent with the generally higher speeds of the spalls.

3.4. Triton

Thus far we have found that launch speed affects ejecta decay somewhat, but that different ejection angles or locations do not matter as much. However, all of our runs so far simulate the rather complicated Jupiter and Saturn systems; this tends to obscure the competing influences of multiple perturbers and targets. The better to separate various effects, we decided to perform new simulations of a much simpler system, consisting only of Neptune and Triton, its largest moon by far.

Triton's orbit is notably circular; in fact, its eccentricity is essentially undetectable, so we neglected it in all cases. In order to test the effects of three other parameters, we built up a realistic Neptune–Triton system from simpler models in a sequence of eight simulations. Table 8 lists the parameters of these runs, along with the results of fitting their decay curves to laws (1)–(6).

For half of the runs (tabulated in columns 7–10), Triton was given its proper radius of 1352.6 km, GM of 1427.9 km^3/s^2, and escape velocity V_e of 1.4530 km/s. Particles were ejected with a launch speed 1.5000 km/s $= 1.0323 V_e$, leaving a residual speed of 372.4 m/s after escape, small compared to Triton's orbital speed of 4.360 km/s. For the other four simulations (listed in columns 3–6 of Table 6), we launched ejecta at a speed of 372.4 m/s from a Triton with its true radius, but zero mass, as in the case of the massless Hyperion in Table 1. In each of these massless cases, Triton could not scatter its own ejecta, but passively re-accreted all of them with its geometric cross-section alone.

For two of the massless Triton runs, and for two of the massive Triton runs (columns 3, 4, 7, and 8 of Table 8), we neglected Neptune's oblateness. In the absence of this or other perturbations, the Neptune–Triton–particle system thus constitutes a Circular Restricted Three-Body Problem (CR3BP). Under such conditions the Jacobi constant (analogous to energy, and often approximated as the Tisserand parameter) is conserved; this ensures that a given ejectum approaches Triton with the same speed at each close encounter.

For the other four simulations (columns 5, 6, 9, and 10 of Table 8), Neptune was given its proper radius of 25,225 km and true dynamic oblateness $J_2 = 0.0034105$. This perturbation causes the orbits of ejecta to precess with periods of $\sim$700 years about Neptune's equator plane, inclined by $\sim 156^\circ.8$ ($23^\circ.2$ retrograde) to Triton's orbit. This breaks the Jacobi constant and allows a particle to re-encounter Triton with a somewhat different speed each time.

For each combination of mass and oblateness, we launched 360 particles vertically from 360 equally spaced points along Triton's equator, taken as coincident with its orbital plane (columns 3, 5, 7, and 9 of Table 8). If the oblateness is zero as well, then the ejecta must always remain in Triton's orbital plane; this reduces the problem to two dimensions and dra-

Table 5
Fit parameters of various decay laws for ejecta from Ganymede

	Launch speed	$0.96V_e$	$0.98V_e$	$1.00V_e$	$1.20V_e$	$1.40V_e$	Vertical
	Run time (yr)	19,299	62,501	100,000	54,822	100,000	45,117
	Initial particles T	119	166	178	179	180	147
Decay law	Final particles	0	0	1	0	1	0
Simple	D	0.169	0.155	0.156	0.0437	0.0481	0.0693
power	C/T	0.655	0.678	0.752	0.948	0.967	0.910
law (1)	χ	3.115	4.158	2.991	5.419	5.144	4.199
	t_0 (yr)	0.0807	0.0813	0.160	0.296	0.494	0.257
Shifted	D	0.236	0.234	0.196	0.0674	0.0727	0.0980
power	T_*/T	1.203	1.194	1.156	1.065	1.073	1.090
law (3)	χ	1.968	2.548	2.307	5.227	4.904	3.810
Simple	B/T	0.193	0.184	0.179	0.200	0.201	0.198
logarithmic	A/T	0.748	0.768	0.817	0.914	0.962	0.896
law (2)	t_{00} (yr)	7.5×10^3	1.5×10^4	3.6×10^4	3.8×10^4	6.0×10^4	3.4×10^4
	χ	3.838	7.102	4.493	6.781	6.244	3.834
	t_0 (yr)	0.0492	0.0548	0.0953	0.371	0.647	0.298
Shifted	B/T	0.197	0.188	0.182	0.221	0.222	0.217
logarithmic	T_*/T	1.021	1.023	1.016	1.091	1.094	1.080
law (4)	t_{00} (yr)	7.4×10^3	1.5×10^4	3.6×10^4	3.2×10^4	5.4×10^4	2.9×10^4
	χ	4.101	7.548	4.804	5.353	4.834	2.805
Simple	t_0 (yr)	5005	19,186	23,538	8825	15,219	8570
exponential	T_*/T	0.108	0.0527	0.0919	0.326	0.319	0.299
decay (5)	χ	1.239	1.408	1.506	2.388	2.300	1.824
Stretched	t_0 (yr)	23.69	23.06	106.4	600.0	1138	590.6
exponential	β	0.280	0.283	0.300	0.497	0.499	0.433
decay (6)	χ	1.925	1.751	1.558	1.768	1.407	0.954
	t_E (yr)	10.49	14.76	60.75	406.8	733.3	449.5

matically increases the rate of re-accretion. Finally, for each combination of mass and oblateness, we also launched 360 particles vertically from 360 equally spaced points along Triton's 45° north parallel of latitude (columns 4, 6, 8, and 10). This gives the ejecta an inclination with respect to Triton's orbit, and restores the problem to three dimensions.

We begin with the simplest case, equatorial ejection when Triton's mass and Neptune's oblateness both vanish (column 3 of Table 8). Decay is very rapid in this non-scattering, two-dimensional case, as shown both by t_E and by the total run time. None of the logarithmic or power laws (1)–(4) seems to fit this case very well. However, both the simple and stretched exponential laws (5) and (6) fit quite well: $t_0 \approx t_E$ for both laws, and both have fitness measures χ of about unity. Furthermore, $T_*/T \approx 1$ as well for the simple exponential law (5), signifying a realistic fit. Finally, the stretching parameter β (given with its one-sigma uncertainty in Table 8) also is nearly indistinguishable from unity for the stretched exponential law (6), implying that it closely approximates simple exponential decay (5).

Fig. 9 displays the decay curves for the above case, in the usual format. Note that now the green curve is closest to the diagonal; this confirms that the decay curve for this case is nearly a pure exponential. From this it is tempting to conclude that the process of re-accretion is random, such that each ejecta particle has the same probability of removal per unit time. However, examination of the particle lifetimes versus the longitude of launch (cf. Fig. 1 of Dobrovolskis and Lissauer, 2004) reveals that ejecta from Triton's leading and trailing quadrants are re-accreted in about half the time as those from its sub-Neptune and anti-Neptune quadrants. Thus the removal probability per unit time is not constant, but a systematic function of launch circumstances.

A similar pattern arises for midlatitude ejection when Triton's mass and Neptune's oblateness both vanish (column 4 of Table 8), but the other simulations cannot be characterized in any such simple manner. Examination of column 4 in Table 8 shows that this three-dimensional case is not fit by simple exponential decay (5) much better than by the power or log laws (1)–(4). Furthermore, although the fitness measure χ is acceptable for the Kohlrausch law (6), the best-fit exponent β is significantly greater than unity, as in *compressed* exponential decay. On the face of it, this suggests a process of diffusion, similar to a random walk. However, no diffusion can occur in this simulation, any more than in the previous case, because a massless Triton cannot scatter its ejecta; since Neptune's oblateness is also neglected, the particle orbits cannot even precess, but must remain fixed.

In fact, Fig. 10 (in the usual format) reveals that the decay curve for this case is nearly *linear* in time, corresponding neither to the diffusion solution (8), nor to any of our proposed

Table 6
Fit parameters of various decay laws for spalls from Io

	Location	Apex	Sub-jovian	Anti-jovian	Pole	Combined
	Initial particles T	572	546	539	568	2225
Decay law	Final particles	3	2	4	4	13
Simple power law (1)	D	0.153	0.120	0.103	0.162	0.0996
	C/T	0.650	0.634	0.677	0.590	0.682
	χ	6.560	7.457	8.160	6.590	16.871
	t_0 (yr)	0.0600	0.0222	0.0225	0.0384	0.0215
Shifted power law (3)	D	0.204	0.172	0.154	0.218	0.152
	T_*/T	1.166	1.143	1.127	1.176	1.123
	χ	5.827	6.117	6.758	5.414	13.745
Simple logarithmic law (2)	B/T	0.245	0.224	0.228	0.237	0.225
	A/T	0.681	0.623	0.624	0.647	0.625
	t_{00} (yr)	595.0	601.7	549.5	533.4	590.2
	χ	5.701	6.365	6.886	6.237	14.111
	t_0 (yr)	0.0499	0.0208	0.0224	0.0324	0.0216
Shifted logarithmic law (4)	B/T	0.257	0.238	0.246	0.250	0.243
	T_*/T	1.047	1.060	1.072	1.050	1.072
	t_{00} (yr)	583.2	582.7	514.6	521.8	553.1
	χ	6.201	6.401	6.215	6.965	12.387
Simple exponential decay (5)	t_0 (yr)	158.8	150.6	176.8	179.0	159.2
	T_*/T	0.338	0.303	0.320	0.277	0.349
	χ	3.729	3.481	4.281	3.807	8.360
Stretched exponential decay (6)	t_0 (yr)	13.862	9.434	10.614	8.952	10.662
	β	0.464	0.432	0.447	0.420	0.441
	χ	1.882	2.384	2.529	2.683	4.831
	t_E (yr)	5.526	3.486	3.987	2.909	3.911

Note. All runs lasted 1000 years.

decay laws (1)–(6). For comparison, fitting this decay curve to a linear decay law

$$S(t) = T_*[1 - t/t_{00}] \tag{11}$$

gives a relatively high fitness measure $\chi = 5.713$, but a reasonable initial number $T_* = 334.2 \pm 6.1$ compared to the actual total $T = 360$, and a realistic extinction time $t_{00} = 23.80 \pm 0.54$ yr at which all of the particles are gone, compared to the actual run time of 24.99 yr.

Columns 5 and 6 of Table 8 show the effect of Neptune's oblateness on the two previous cases. The decay times are much longer in both cases, but now the latitude of ejection makes little difference between them. The decay curve corresponding to column 5 is graphed in Fig. 11, in the by-now familiar format. The corresponding plot for column 6 is very similar; both resemble Figs. 1 and 3–8 more than the "pathological" cases in Figs. 9 and 10. Table 8 implies that the simple or stretched exponential law fits these cases best, while Fig. 11 favors the logarithmic (blue) or stretched exponential (red) law.

Column 7 of Table 8 shows the effects of Triton's mass on the planar case of equatorial ejection without oblateness. In this simulation, Triton managed to expel one particle from the Neptune–Triton system by a series of distant encounters, but it re-accreted all of the others. The gravitational enhancement of Triton's collisional cross-section accelerates the initial decay, as shown by the decreases in t_E and in t_0 for the stretched exponential law (6) from the massless case in column 3. However, gravitational scattering by Triton "stretches" the tail of the decay curve, as shown by the increases in total run time and in t_0 for the simple exponential law (5). Fig. 12 displays the decay curve corresponding to this case. Both Fig. 12 and column 6 of Table 8 show that none of our decay laws (1)–(6) gives a particularly good fit to this simulation.

The corresponding plots for the other massive simulations (columns 8–10 in Table 8) generally resemble Fig. 12, except for time-scale. As Table 8 shows, Neptune's oblateness and non-equatorial launch both lengthen all relevant time-scales. Note that columns 7 and 9 list time shifts t_0 for the shifted log law (4) even shorter than Triton's orbital period 5.877 days = 0.0161 yr. In fact, including t_0 causes a slight degradation of the log fits for all four massive Triton runs, as it did for low-speed ejecta from Ganymede (Table 5). Finally, the sixth row of Table 8 shows that Triton expelled a few particles from the Neptune–Triton system in each massive case. All of the others hit Triton; no ejecta ever reached Neptune itself, which would require still stronger perturbations.

4. Discussion

We have seen that in gravitational systems dominated by a central mass, the decay curves of small bodies initially in secondary-crossing orbits usually are fit best by the generalized

Table 7
Fit parameters of various decay laws for rubble from Io

	Location	Apex	Sub-jovian	Anti-jovian	Pole	Combined
	Run time (yr)	1000	1000	592.1	1000	1000
	Initial particles T	559	436	442	531	1968
Decay law	Final particles	3	4	0	2	9
Simple power law (1)	D	0.180	0.163	0.199	0.265	0.140
	C/T	0.551	0.543	0.504	0.423	0.582
	χ	5.700	6.513	5.884	4.291	15.606
	t_0 (yr)	0.0368	0.0234	0.0319	0.0391	0.0211
Shifted power law (3)	D	0.235	0.236	0.281	0.342	0.217
	T_*/T	1.184	1.195	1.229	1.271	1.170
	χ	4.541	4.604	4.451	3.096	11.188
Simple logarithmic law (2)	B/T	0.235	0.230	0.240	0.225	0.228
	A/T	0.644	0.609	0.604	0.596	0.613
	t_{00} (yr)	546.2	441.4	331.6	450.1	488.0
	χ	6.317	6.411	9.056	11.132	16.536
	t_0 (yr)	0.0305	0.0200	0.0223	0.0160	0.0201
Shifted logarithmic law (4)	B/T	0.247	0.243	0.247	0.225	0.244
	T_*/T	1.047	1.052	1.031	1.002	1.065
	t_{00} (yr)	540.0	429.5	331.2	452.1	477.3
	χ	7.253	7.050	9.956	11.651	17.951
Simple exponential decay (5)	t_0 (yr)	158.6	218.5	75.5	163.2	143.0
	T_*/T	0.280	0.214	0.294	0.172	0.345
	χ	3.632	3.431	3.315	3.327	8.599
Stretched exponential decay (6)	t_0 (yr)	7.476	4.901	3.396	2.891	4.489
	β	0.398	0.363	0.428	0.375	0.384
	χ	2.220	3.165	3.013	2.960	5.721
	t_E (yr)	5.477	2.648	2.143	1.859	2.712

exponential law (6), where the stretching parameter β generally ranges between about $1/2$ and $1/3$. Furthermore, the e-folding time t_e of satellite ejecta grows as the $1-\beta$ power of the elapsed time t, ranging from $\sim 1/2$ to $\sim 2/3$. We attribute this lengthening of t_e to a combination of two effects, which we call "spreading" and "culling."

Spreading is analogous to a process of diffusion. For example, displacement in a random walk increases as $t^{1/2}$, corresponding to normal or Fickian diffusion. However, chaotic physical systems can display "strange kinetics," where displacements grow as some other power of the time, t^{μ} (Shlesinger et al., 1993). If $\mu > 1/2$, the system is called "super-diffusive"; if $\mu < 1/2$, it is called "sub-diffusive" (Morbidelli and Froeschlé, 1996). For instance, Petit and Hénon (1987) find that, without shepherding, a narrow planetary ring broadens sub-diffusively, as $t^{1/3}$ ($\mu = 1/3$).

In the situations treated in this paper, the particle population spans a narrow range of orbits at first, but spreads into a wider range over the course of time. Some of the particles "hide" for long intervals in relatively safe niches, such as temporary resonances with the planets or satellites, while other new orbits are relatively dangerous and short-lived, like planet-crossing asteroids.

Probably the most important spreading mechanism is dynamical heating. This refers to the gradual rise in eccentricities, inclinations, and velocities of particles (relative to their sources and sinks). In many respects it resembles a process of diffusion in the space of orbital elements. Particle time constants gradually lengthen as ejecta spread away from their source bodies, which are also their dominant sinks (except that Titan is the main sink for ejecta from nearby Hyperion).

Figs. 2–4 of Dobrovolskis and Lissauer (2004) show how dynamical heating gradually spreads ejecta from Hyperion throughout the Saturn system. Comparison of the massive and massless Hyperion results from Table 3 of that paper and from Table 1 of this one indicates that Hyperion itself is the initial source of this heating, despite its small size, but also that other perturbations (mainly from Titan) are important as well.

Similarly, Fig. 7 of Gladman et al. (1995) and Fig. 2 of Gladman et al. (1996) graphically show dynamical heating of lunar ejecta, while Fig. 4 of Gladman et al. (1996) and Fig. 3 of Gladman (1997) do the same for martian ejecta. Wetherill (1977, Fig. 4) dramatically cartoons spreading of planetesimals left over from the accretion of the Earth.

The primary cause of spreading is gravitational scattering, but orbital precession can also cause dynamical heating. Comparison of columns 5 and 6 of Table 8 with columns 3 and 4 shows how including Neptune's dynamical oblateness stretches the decay of ejecta from Triton.

Culling refers to the case when the initial particle population spans a wide range of orbits, some of which are more prone to removal than others (e.g., low vs high inclinations).

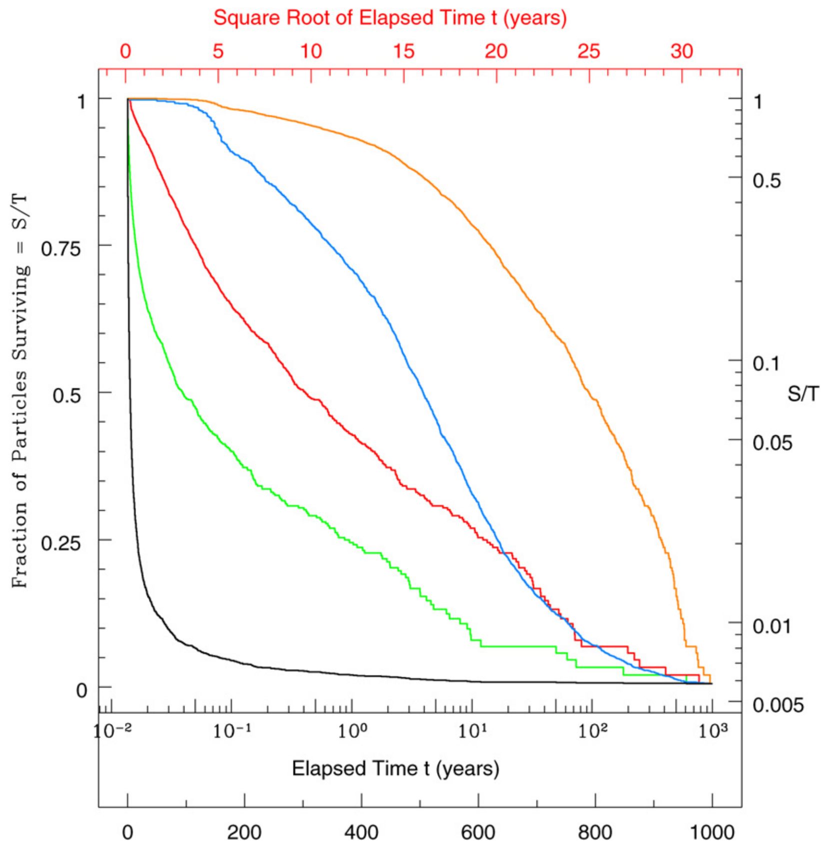

Fig. 8. Comparison of decay laws for spalls from Io. Format similar to Fig. 1.

The more "endangered" particles tend to be removed first, just as predators cull slower, weaker prey from the herd, or as orchard workers make short work of picking low-hanging fruit.

As yet another analogy, imagine analyzing an unknown mixture of radioactive wastes. Suppose that the waste contains only two unstable nuclides with different time constants, and that all daughter nuclei are stable, so that there are no decay chains. Then the combined decay curve of the mix is the sum of two simple exponentials. As the specimen decays, the population of both radionuclides declines, but the ratio of long-lived to short-lived nuclei increases, and the effective e-folding time t_e of the whole sample grows with time.

In fact, Wetherill (1979) has shown that a simple two-compartment model of Earth-crossing and Mars-crossing asteroids yields a population of Earth-crossers which decays as the sum of two simple exponentials (plus a constant term, if a steady-state source is operating; see Appendix B). If the two time constants were sufficiently different, the net decay curve would resemble two straight lines in a log:linear plot (like the green curves in Figs. 1 and 3–12): an initially steep slope dominated by the short-lived component, followed by a slow tail dominated by the long-lived one. Note that none of our green curves looks quite like this.

More generally, the net decay curve can be viewed as a linear combination (with positive coefficients) of many simple exponential decays of the form $\exp(-kt)$. Unlike a mixture of radioactive nuclides, though, the distribution of particle orbits can be considered to contain a continuous distribution F of decay constants k. How can $F(k)$ be recovered? It turns out that the decay curve S/T or $f(t)$ is the Laplace transform of the desired distribution F of time constants; thus F is just the inverse Laplace transform of f. $F(k)$ may be regarded as the "Laplace spectrum" of the decay curve, analogous to the Fourier spectrum of a periodic function.

Like most inverse problems, "Laplace analysis" is generally difficult. Closed-form expressions (Oberhettinger and Badii, 1973) are known for the Laplace spectra of the power laws (1) and (3), and for the Kohlrausch law (6) in the particular cases $\beta = 1/3$ and $\beta = 1/2$ (stretched exponential decay), as well as for $\beta = 1$ (simple exponential decay). For example, the spectrum of simple exponential decay (5) is a Dirac delta-function at the unique time constant t_0. However, it can be shown that any linear combination of exponential decay curves *with positive coefficients* must be concave upwards everywhere. Therefore no Laplace spectrum (with non-negative amplitudes) can exist for compressed exponential decay ($\beta > 1$), the diffusion solution (10), nor either logarithmic law (2) or (4).

Matrix methods exist to Laplace-analyze decay curves like ours computationally. Unfortunately, such algorithms are numerically ill-conditioned (Bellman et al., 1966), and rather unstable in practice. Spreading also alters particle orbits with time, which renders Laplace spectra less meaningful. Despite these problems, we attempted to recover Laplace spectra from our decay curves by using the publicly available Matlab script reginvlaplace.m (Rogers, 2005). However, the results were disappointing and are not presented here.

Table 8
Fit parameters of various decay laws for Triton ejecta

	GM of Triton	0				1427.9 km^3/s^2			
	J_2 of Neptune	0		0.0034105		0		0.0034105	
	Launch latitude	0	45°	0	45°	0	45°	0	45°
	Run time (yr)	19.08	24.99	828.1	855.6	2364	33,634	17,242	34,612
	Initial particles T	359	360	359	360	357	359	357	359
Decay law	Particles expelled	0	0	0	0	1	8	6	16
Simple	D	0.0866	0.0493	0.118	0.0746	0.244	0.144	0.249	0.158
power	C/T	0.794	0.912	0.736	0.877	0.470	0.728	0.464	0.706
law (1)	χ	6.571	6.032	5.579	6.656	5.143	5.695	4.274	5.237
	t_0 (yr)	0.0700	0.153	0.0754	0.173	0.0453	0.110	0.0461	0.110
Shifted	D	0.142	0.0857	0.168	0.122	0.363	0.193	0.331	0.205
power	T_*/T	1.119	1.071	1.144	1.106	1.300	1.159	1.269	1.169
law (3)	χ	6.295	5.913	4.568	5.761	4.045	5.016	2.757	4.288
Simple	B/T	0.418	0.373	0.257	0.279	0.199	0.189	0.176	0.183
logarithmic	A/T	0.555	0.732	0.716	0.804	0.536	0.764	0.644	0.780
law (2)	t_{00} (yr)	21.30	91.32	611.2	763.9	496.4	11,215	4476	17,961
	χ	10.18	15.41	4.338	8.094	22.74	10.28	14.59	7.228
	t_0 (yr)	0.0864	0.191	0.0788	0.199	0.00461	0.0560	0.00945	0.0634
Shifted	B/T	0.506	0.504	0.281	0.314	0.196	0.190	0.175	0.186
logarithmic	T_*/T	1.182	1.186	1.084	1.113	0.989	1.008	0.991	1.015
law (4)	t_{00} (yr)	18.6	42.6	572.8	698.4	498.0	11,238	4510	17,935
	χ	6.754	11.88	3.332	5.138	22.83	10.75	14.77	7.690
Simple	t_0 (yr)	4.238	10.54	123.3	114.2	375.2	7652	4904	7651
exponential	T_*/T	1.015	1.049	0.536	0.813	0.166	0.0775	0.0435	0.130
decay (5)	χ	1.036	3.469	2.476	1.773	2.757	2.195	1.444	1.381
Stretched	t_0 (yr)	4.343	10.75	25.52	57.15	1.919	40.60	3.830	52.13
exponential	β	1.029	1.306	0.479	0.610	0.413	0.364	0.273	0.301
decay (6)		±0.026	±0.037	±0.017	±0.026	±0.035	±0.020	±0.015	±0.014
	χ	0.960	1.473	2.316	2.411	4.065	3.091	3.911	3.584
	t_E (yr)	4.232	11.42	38.99	93.36	1.489	24.97	1.813	24.66

Note. No particles survived.

The relative importance of spreading versus culling remains an open question. The role of culling is not clear in our Triton simulations, because all of the ejecta were launched with the same speed. However, spreading was definitely absent in the massless Triton cases where Neptune's oblateness was neglected too (Figs. 12 and 13, and columns 3 and 4 of Table 8). In these two runs, ejecta decay assumes a simple or even compressed exponential form. In contrast, both spreading and culling must operate in the Öpik-type simulation of near-Earth objects by Gladman et al. (2000, Fig. 2). Nevertheless, their decay curve is well fit by a simple exponential decay of the form $2^{-t/60\ \mathrm{Myr}} \approx \exp(-t/87\ \mathrm{Myr})$.

Figs. 17 and 18 of Alvarellos et al. (2002) and Figs. 5, 9, 11, and 13 of Alvarellos et al. (2005) show how the relative velocity at which ejecta hit satellites increases as a function of time. This too can be attributed to a combination of spreading and culling. However, Fig. 14 of Alvarellos et al. (2005) also reveals that rubble from Mimas does not spread far from its orbit. Thus culling appears more important than spreading, at least for Mimas ejecta.

It is noteworthy that our decay curves resemble the distribution of crater ages on the Moon, with a steep spike near 3.9 Gyr ago corresponding to the so-called lunar cataclysm or late heavy bombardment, followed by a more gradual decline to the present day (e.g., Hartmann, 1972; Hartmann et al., 2000). Indeed, Dones et al. (1999b) have suggested that the planetesimals left over from the accretion of the Earth and Moon decayed according to a simple logarithmic law like Eq. (2). Gladman et al. (1995, 1996) and Gladman (1997) also have developed an interesting application of their decay curves to the ages of meteorites from the Moon and Mars, as follows.

Impacts by comets and asteroids on the surfaces of the planets and of their satellites produce "primary" craters and eject rocks at a range of velocities. Those ejecta with speeds less than the target's escape velocity follow suborbital trajectories and promptly return to the surface of the parent body, producing "secondary" impacts and associated features. However, ejecta with somewhat higher speeds may escape from the Moon (or another satellite), but remain in orbit about the Earth (or primary planet) for years. Such intermediate ejecta eventually may be expelled from the Earth–Moon system (or whatever), or be re-accreted by the satellite or by the planet itself. We call such impacts "poltorary," from the Slavic word for 3/2, because

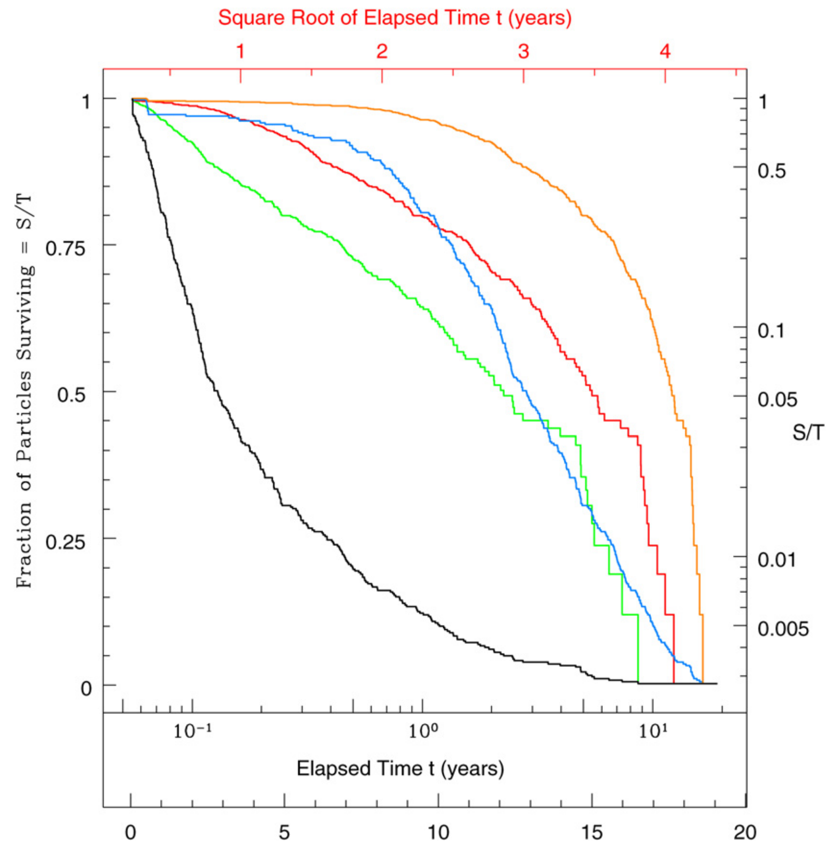

Fig. 9. Comparison of decay laws for equatorial ejecta from massless Triton, without oblateness. Format similar to Fig. 1.

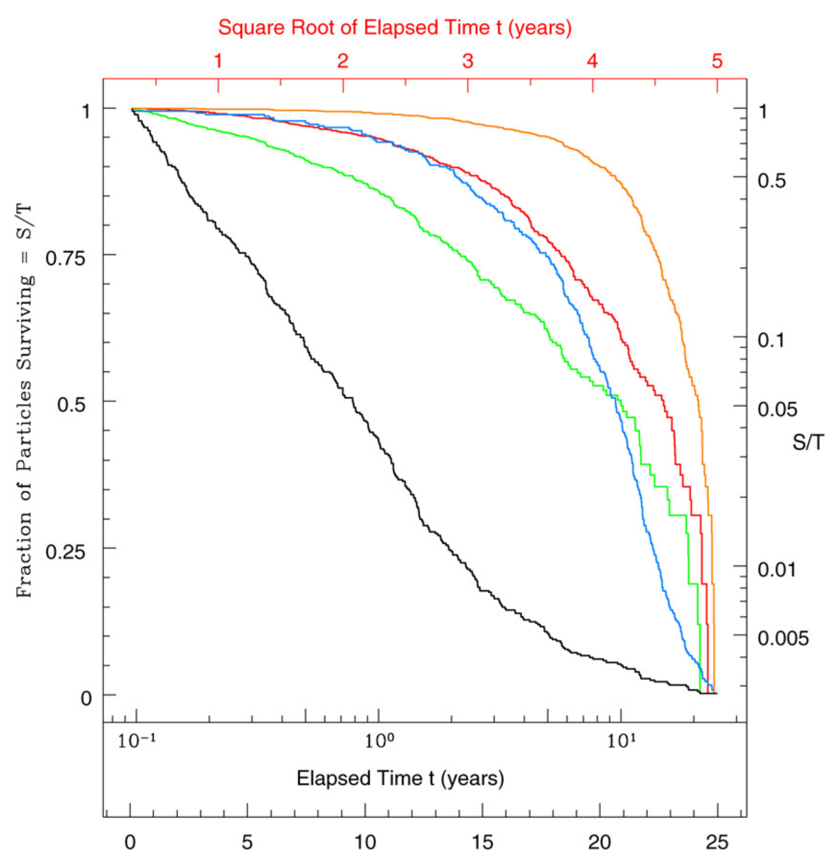

Fig. 10. Comparison of decay laws for midlatitude ejecta from massless Triton, without oblateness. Format similar to Fig. 1.

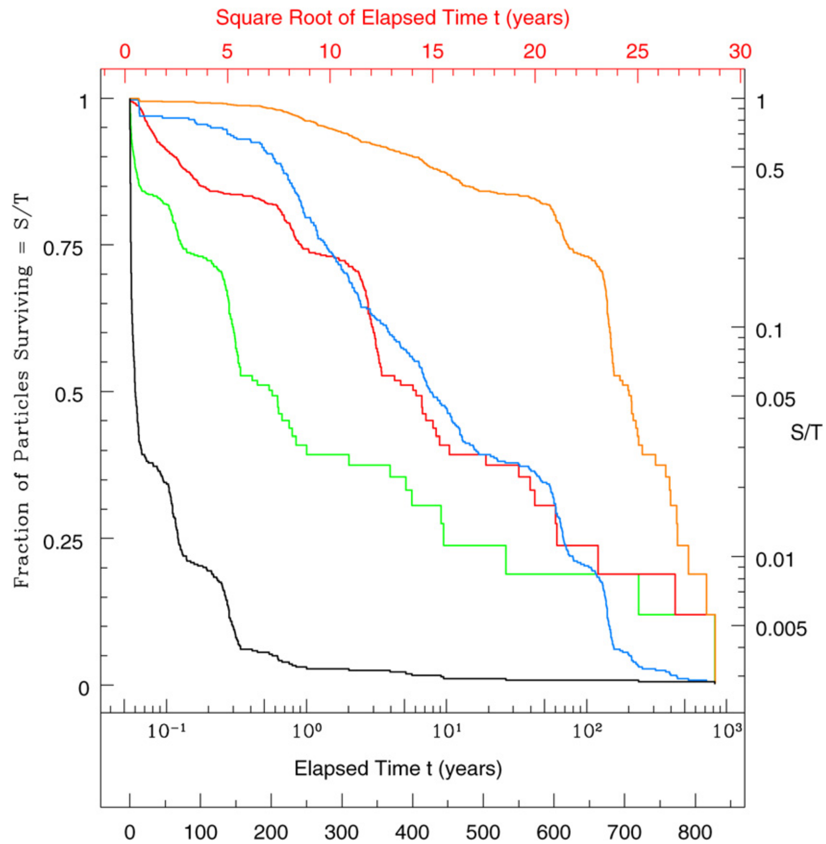

Fig. 11. Comparison of decay laws for equatorial ejecta from massless Triton, with oblateness. Format similar to Fig. 1.

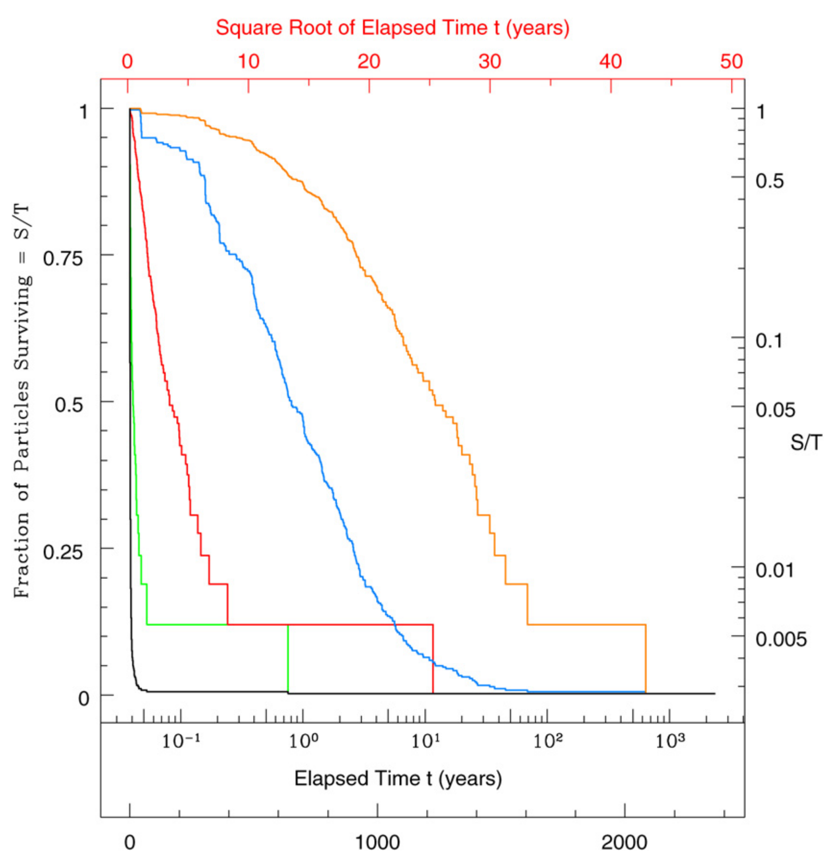

Fig. 12. Comparison of decay laws for equatorial ejecta from massive Triton, without oblateness. Format similar to Fig. 1.

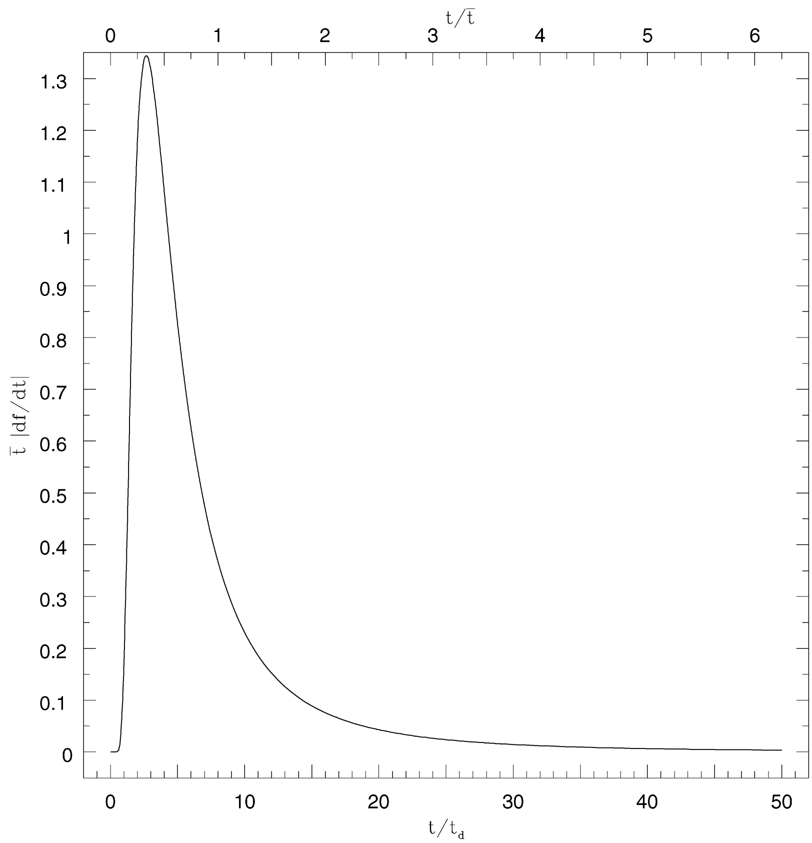

Fig. 13. Lifetime distribution for diffusion solution.

they are intermediate between primary and secondary impacts (Dobrovolskis and Lissauer, 2004; Alvarellos et al., 2005).

In any case, ejecta with the highest speeds escape to heliocentric orbit, to join the population of primary projectiles. Gladman et al. (1995, 1996) found that lunar meteorites in geocentric orbit lasted only a few years before crashing to Earth, but those in heliocentric orbit took some few thousands to millions of years. Eventually some of these find their way into earthly meteorite collections, where dating techniques can determine their "4π" cosmic-ray exposure ages, interpreted as the length of time which these stones spent in free space.

Now the distribution of these ages is equivalent to the distribution of ejecta lifetimes in simulations like ours. As discussed in Appendix B, the distribution of particle lifetimes is just the absolute derivative of the decay curve: $|(\mathrm{d}/(\mathrm{d}t))f(t)| = -(\mathrm{d}/(\mathrm{d}t))f(t)$. By the same token, the decay curve $f(t)$ is also the cumulative distribution of particle lifetimes greater than t. This permits a direct comparison between our decay laws and the cosmic-ray ages of meteorites.

Plotting the 4π ages of the fourteen lunar meteorites from Table 1 of Gladman et al. (1996) in the formats of our Fig. 1 and Figs. 3–12 gives the impression that they fit a power law or logarithmic decay law nicely. In contrast, the corresponding plot for the twelve martian meteorite ages from Table 1 of Gladman (1997) suggests that they follow a linear or simple exponential decay law instead. Fitting both cumulative age distributions to our decay laws (1)–(6) also seems to give plausible values for χ and for the fit parameters; however, their uncertainties are so large as to be essentially meaningless. Apparently on the order of 100 dates are required for meaningful fits, rather than only a dozen or so. We leave this task to the future.

5. Conclusions

Small bodies left over from the formation of the planets and satellites litter the Solar System. Along with the debris from more recent collisions, these bodies are removed by expulsion from heliocentric or planetocentric orbit, as well as by collisions with planets, moons, and the Sun, with characteristic lifetimes depending on their orbits. The rate at which a given population of objects is removed is poorly described by the simple exponential law used to describe radioactive decay. On the contrary, the removal of comets and remnant planetesimals has sometimes been described as "logarithmic decay" or as power law decay.

Our work suggests that the removal of ejecta from planetary satellites is best described by none of the above, but by a "stretched exponential" decay law of the form $\exp(-[t/t_0]^{\beta})$. Under this law, the particle lifetimes increase as a fractional power $0 < 1 - \beta < 1$ of the elapsed time t.

Statistical analysis enables us to determine the decay parameters, and supports the stretched exponential model, which suggests some sort of diffusion process. Our results may be applicable in several contexts, including the delivery of meteorites to Earth and the bombardment histories of the planets and their moons.

Acknowledgments

We are obliged to Kevin Zahnle, Patrick Hamill, and Salman Rogers for fruitful discussions. We also thank Zahnle, Hamill, and Doug Hamilton for previewing the manuscript, and Luke Dones for reviewing it. A.R.D. and J.J.L. were supported by NASA's Planetary Geology and Geophysics Program through RTOP 344-30-50-01, while J.L.A. was supported by NASA's Outer Planet's Research Program.

Appendix A. Least-squares fits and uncertainties

First we require a measure of the uncertainty of the number $S(t)$ of particles surviving at a given elapsed time t. Let $R(t)$ be the number of particles removed to date by all mechanisms, and let $T \equiv S(0)$ be the total number of particles in the simulation. Note $R + S = T$ at any time. Now assume that each particle has a certain probability $p(t)$ of having been removed already by any means, and has the complementary probability $1 - p$ of having survived thus far. In a large number of independent trials, this process would lead to a binomial distribution of removals

$$\binom{T}{R} p^R (1-p)^S = T! \frac{p^R}{R!} \frac{(1-p)^S}{S!} \tag{A.1}$$

whose mean is Tp and whose variance is $Tp(1-p)$ (Bevington and Robinson, 1969). Our best estimate for the probability of removal by time t is just $p = R/T$, so the variance of the R distribution (A.1) becomes $R(1 - R/T) = R(T - R)/T = RS/T$, symmetrical in R and S. Taking the square root of this variance, we obtain the standard deviation

$$\sigma = \sqrt{RS/T}. \tag{A.2}$$

Note that σ is the uncertainty both in the number S of survivors and in the number R of removals to date. For small R/T, σ reduces to $\sqrt{R}$ as in simple counting statistics; similarly σ tends to $\sqrt{S}$ for small S/T. Furthermore, $R \pm \sigma$ and $S \pm \sigma$ never go negative or exceed T. Also note that $\sigma > 1$ except for the first and last few removals, so that the uncertainty exceeds the shot noise associated with the discrete steps in the decay curves.

Now we wish to fit straight lines of the form $mx + b$ to our decay curves $y(x)$. In the present context, the independent variable x may be t, $\log t$, or $\log(1 + t/t_0)$, while the dependent variable y may be S, $\log S$, or $\log(-\ln(S/T))$. If $y = S$, then the uncertainty (standard deviation) in y is $\sigma(y) = \sigma(S) = \sqrt{RS/T}$, from Eq. (A.2). In the case $y = \log S$, $\sigma(y) = \sigma(S)|\mathrm{d}y/\mathrm{d}S| = \sigma(S)\frac{\mathrm{d}}{\mathrm{d}S}\log S = \sqrt{RS/T}\log(e)/S \approx 0.4343\sqrt{R/(ST)}$. When $y = \log|\ln(S/T)|$, $\sigma(y) = \sigma(S)|\frac{\mathrm{d}}{\mathrm{d}S} \times [\log|\ln(S/T)|]| = \sqrt{RS/T}\log(e)/|S\ln(S/T)| \approx \frac{0.4343}{|\ln(S/T)|} \times \sqrt{R/(ST)}$.

Finding the best-fitting straight line is equivalent to minimizing

$$\chi^2(m,b) \equiv \frac{1}{W}\int \frac{[mx + b - y(x)]^2}{\sigma^2(y)}\,\mathrm{d}x, \tag{A.3}$$

the weighted integral of squared differences between the line and the curve. Here we have normalized χ^2 above by $W \equiv \int \mathrm{d}x$ to account for the continuous nature of the data. Note that χ^2 as defined above is a continuum version of the more familiar discrete statistic χ_ν^2, the reduced chi-square (Bevington and Robinson, 1969). In simple terms, $\chi \equiv \sqrt{\chi^2}$ is a measure of the deviation of the fit from the curve, in units of σ. For example, a curve which always lies within three standard deviations of the best-fitting straight line must have $\chi < 3$ (although the converse does not hold). A really good fit should have $\chi \lesssim 1$.

The decay curve $y(x)$ is piecewise constant (like a stairway), and so is its variance $\sigma^2(y)$. Then if we write y_i for the value of y between successive particle removals at $x = x_i$ and x_{i+1}, we can express χ^2 above in terms of sums rather than as an integral:

$$W\chi^2(m,b) = m^2 Z_{xx} + 2mbZ_x + b^2 Z - 2mZ_{xy} - 2bZ_y + Z_{yy}, \tag{A.4}$$

where we define

$$Z \equiv \sum_i \frac{x_{i+1} - x_i}{\sigma^2(y_i)}, \quad Z_x \equiv \sum_i \frac{x_{i+1}^2 - x_i^2}{2\sigma^2(y_i)},$$
$$Z_{xx} \equiv \sum_i \frac{x_{i+1}^3 - x_i^3}{3\sigma^2(y_i)}, \quad Z_y \equiv \sum_i \frac{[x_{i+1} - x_i]y_i}{\sigma^2(y_i)},$$
$$Z_{xy} \equiv \sum_i \frac{[x_{i+1}^2 - x_i^2]y_i}{2\sigma^2(y_i)}, \quad Z_{yy} \equiv \sum_i \frac{[x_{i+1} - x_i]y_i^2}{\sigma^2(y_i)}. \tag{A.5}$$

Because $\sigma^2(y)$ vanishes for $R = 0$, these sums begin only with the first removal. In principle, they continue until the removal of the last particle, but in practice they continue only until the end of the simulation.

In order to minimize χ^2, we first differentiate Eq. (A.4) with respect to m and b:

$$W\frac{\partial\chi^2}{\partial m} = 2mZ_{xx} + 2bZ_x - 2Z_{xy}, \tag{A.6}$$

$$W\frac{\partial\chi^2}{\partial b} = 2mZ_x + 2bZ - 2Z_y. \tag{A.7}$$

Next we set the above partial derivatives equal to zero, to obtain the equations of condition. Solving the resulting simultaneous linear equations for m and b then gives

$$m = \frac{ZZ_{xy} - Z_x Z_y}{\Delta} \quad \text{and} \quad b = \frac{Z_{xx}Z_y - Z_x Z_{xy}}{\Delta}, \tag{A.8}$$

where $\Delta \equiv Z_{xx}Z - Z_x^2$.

Finding the uncertainty in these parameters is trickier, but from Eqs. (A.5) and (A.8) we find

$$\begin{aligned}\sigma^2(m) &= \sigma^2\left(\sum_i\left[Z\frac{x_{i+1}^2 - x_i^2}{2\sigma^2(y_i)} - Z_x\frac{x_{i+1} - x_i}{\sigma^2(y_i)}\right]\frac{y_i}{\Delta}\right) \\ &= \sum_i\left[Z\frac{x_{i+1}^2 - x_i^2}{2\sigma^2(y_i)} - Z_x\frac{x_{i+1} - x_i}{\sigma^2(y_i)}\right]^2\frac{\sigma^2(y_i)}{\Delta^2} \\ &= \left[Z^2\sigma^2(Z_{xy}) - 2Z_x Z\,\mathrm{cov} + Z_x^2\sigma^2(Z_y)\right]/\Delta^2 > 0\end{aligned} \tag{A.9}$$

and

$$\sigma^2(b) = \sigma^2\left(\sum_i \left[Z_{xx}\frac{x_{i+1}-x_i}{\sigma^2(y_i)} - Z_x\frac{x_{i+1}^2-x_i^2}{2\sigma^2(y_i)}\right]\frac{y_i}{\Delta}\right)$$
$$= \sum_i \left[Z_{xx}\frac{x_{i+1}-x_i}{\sigma^2(y_i)} - Z_x\frac{x_{i+1}^2-x_i^2}{2\sigma^2(y_i)}\right]^2\frac{\sigma^2(y_i)}{\Delta^2}$$
$$= \left[Z_{xx}^2\sigma^2(Z_y) - 2Z_{xx}Z_x\,\mathrm{cov} + Z_x^2\sigma^2(Z_{xy})\right]/\Delta^2 > 0, \tag{A.10}$$

where we define

$$\sigma^2(Z_y) \equiv \sum_i \frac{[x_{i+1}-x_i]^2}{\sigma^2(y_i)},$$
$$\mathrm{cov} \equiv \sum_i \frac{[x_{i+1}-x_i][x_{i+1}^2-x_i^2]}{2\sigma^2(y_i)},$$
$$\sigma^2(Z_{xy}) \equiv \sum_i \frac{[x_{i+1}^2-x_i^2]^2}{4\sigma^2(y_i)}. \tag{A.11}$$

The six sums defined in Eq. (A.5) were evaluated numerically for each model fit and used in Eq. (A.8) to find m and b. Substituting the resulting values back into Eq. (A.4) then gave χ. The three additional sums defined in Eq. (A.11) were also evaluated numerically and used in Eqs. (A.9) and (A.10) to find the variances of m and b. Finally m, b, and their variances were converted back into physical parameters and their uncertainties, as needed.

Appendix B. Lifetime distributions

In order to compare simulations with different total numbers of particles, we need to normalize our decay curves; but first we must distinguish between *stable* and *unstable* sub-populations. Although the number $S(t)$ of particles surviving until time t vanishes as $t \to \infty$ for each of the decay laws considered in this paper (presumably appropriate for satellite-crossing ejecta), it is quite possible for each population to contain a number $S(\infty)$ of stable particles which are never removed (or in practice, survive longer than the simulations). Then the total number of unstable particles is $S(0) - S(\infty)$, while the number of unstable particles surviving until time t becomes $S(t) - S(\infty)$.

Note that $S(0)$ may diverge, as in the simple power law (1) or in the simple logarithmic law (2). Assuming that $S(0)$ exists, we set $T \equiv S(0)$ and define $g \equiv S(\infty)/S(0) = S(\infty)/T$ as the *fraction* of stable particles in the population. We also define $f(t) \equiv [S(t) - S(\infty)]/S(0) = S(t)/T - g$ as the fraction of all particles with lifetimes greater than t, but still finite. Then $f(\infty) = 0$, while $f(0) = 1 - g \equiv f_0$ is the fraction of all unstable particles in the population.

Now the fraction of all particles with lifetimes between t and $t + \mathrm{d}t$ is just $f(t) - f(t + \mathrm{d}t)$, so the distribution function of particle lifetimes is the absolute derivative $|\frac{\mathrm{d}}{\mathrm{d}t}f(t)| = -\frac{\mathrm{d}}{\mathrm{d}t}f(t)$. For example, Fig. 13 graphs the lifetime distribution for the diffusion solution (10); this curve is the absolute derivative of the black (lowest) curve in Fig. 3. Note how $\bar{t}|\mathrm{d}f/\mathrm{d}t|$ peaks at $27/e^3 \approx 1.3443$ when $t = \bar{t}/3$, and declines approximately as t^{-3} thereafter. Thus $\bar{t}/3$ is the *modal* lifetime for the diffusion solution (10). However, a unique mode does not always exist.

The lifetime distribution enables us to find other averages of our particle lifetimes as well. The mean lifetime of all *unstable* particles is just the ratio $\int_0^\infty t|\frac{\mathrm{d}f}{\mathrm{d}t}|\,\mathrm{d}t/\int_0^\infty|\frac{\mathrm{d}f}{\mathrm{d}t}|\,\mathrm{d}t = [-tf|_0^\infty + \int_0^\infty f\,\mathrm{d}t]/[f(0) - f(\infty)] = \int_0^\infty f\,\mathrm{d}t/f_0$ (presuming $tf \to 0$ as $t \to \infty$). Similarly, their root-mean-square (RMS) lifetime is $\sqrt{\int_0^\infty t^2|\frac{\mathrm{d}f}{\mathrm{d}t}|\,\mathrm{d}t/f_0} = \sqrt{\int_0^\infty f \times 2t\,\mathrm{d}t/f_0}$ (presuming $t^2 f \to 0$ as $t \to \infty$). However, note that these averages may not always exist either. For example, the mean lifetime for the diffusion solution (10) is exactly $8t_d \equiv \bar{t}$, but its RMS lifetime diverges. A more robust "average" is the median, which always does exist; it is simply equal to the time when half of the *unstable* particles have been removed ($f(t) = f_0/2$). For example, the median lifetime for the diffusion solution (10) is $\sim 4.7666t_d \approx 0.5958\bar{t}$. For comparison, the time at which $f(t) = f_0/e = 1/e$ is $t_E \approx 6.2253t_d \approx 0.7782\bar{t}$.

The usual measure of the width of a distribution is its standard deviation (SD). It is a very useful fact that the square of the SD is the difference of the squares of the RMS and mean lifetimes. However, this means that the SD diverges whenever the RMS diverges, as for the diffusion solution (10). A more robust measure of width is the inter-quartile range (IQR). For example, $f(t)$ for the diffusion solution (10) falls to $3f_0/4 = 3/4$ when $t \approx 2.9711t_d \approx 0.3714\bar{t}$, and $f(t) = f_0/4 = 1/4$ when $t \approx 8.3222t_d \approx 1.0403\bar{t}$. The IQR is just the difference between these first and third quartiles, $\sim 5.3512t_d \approx 0.6689\bar{t}$.

Table 9
Median, mean, and root-mean-square lifetimes of particles decaying according to the shifted power law (3), along with their standard deviation (SD), inter-quartile range (IQR), and the time t_E at which $f(t) = 1/e$

	D	3	2	1	1/2	1/3
t_E/t_0	$e^{1/D} - 1$	$e^{1/3} - 1 \approx 0.3956$	$\sqrt{e} - 1 \approx 0.6487$	$e - 1 \approx 1.7183$	$e^2 - 1 \approx 6.3891$	$e^3 - 1 \approx 19.0855$
Median t/t_0	$2^{1/D} - 1$	$2^{1/3} - 1 \approx 0.2599$	$\sqrt{2} - 1 \approx 0.4142$	1	3	7
Mean t/t_0	$\frac{1}{D-1}$ for $D > 1$	1/2	1	∞	∞	∞
RMS t/t_0	$\sqrt{\frac{2}{[D-1][D-2]}}$ for $D > 2$	1	∞	∞	∞	∞
SD/t_0	$\frac{1}{D-1}\sqrt{\frac{D}{D-2}}$ for $D > 2$	$\sqrt{3}/2 \approx 0.8660$	∞	∞	∞	∞
IQR/t_0	$4^{1/D} - [4/3]^{1/D}$	$4^{1/3} - [4/3]^{1/3} \approx 0.4868$	$2 - \sqrt{4/3} \approx 0.8453$	$8/3 \approx 2.6667$	$128/9 \approx 14.2222$	$1664/27 \approx 61.6296$

Table 10
Modal, median, mean, and root-mean-square lifetimes of particles decaying according to the Kohlrausch (generalized exponential) distribution (6), along with their standard deviation (SD) and inter-quartile range (IQR)

	β	∞	2	1	1/2	1/3
	$\alpha \equiv 1/\beta$	0	1/2	1	2	3
Modal t/t_0	$[1-\alpha]^\alpha$ for $\alpha < 1$	1	$\sqrt{1/2} \approx 0.7071$	0	0	0
Median t/t_0	$[\ln 2]^\alpha$	1	$\sqrt{\ln 2} \approx 0.8326$	$\ln 2 \approx 0.6931$	$[\ln 2]^2 \approx 0.4805$	$[\ln 2]^3 \approx 0.3330$
Mean t/t_0	$\Gamma(\alpha+1)$	1	$\sqrt{\pi/4} \approx 0.8862$	1	2	6
RMS t/t_0	$\sqrt{\Gamma(2\alpha+1)}$	1	1	$\sqrt{2} \approx 1.4142$	$\sqrt{24} \approx 4.8990$	$\sqrt{720} \approx 26.8328$
SD/t_0	$\sqrt{\Gamma(2\alpha+1) - [\Gamma(\alpha+1)]^2}$	0	$\sqrt{1-\pi/4} \approx 0.4633$	1	$\sqrt{20} \approx 4.4721$	$\sqrt{684} \approx 26.1534$
IQR/t_0	$[\ln 4]^\alpha - [\ln(4/3)]^\alpha$	0	$\sqrt{\ln 4} - \sqrt{\ln(4/3)} \approx 0.6411$	$\ln 3 \approx 1.0986$	$[\ln 4]^2 - [\ln(4/3)]^2 \approx 1.8391$	$[\ln 4]^3 - [\ln(4/3)]^3 \approx 2.6404$

To illustrate further, the modal lifetime is always zero for the power laws, but Table 9 shows the median, mean, and RMS lifetimes of particles decaying according to the shifted power law (3), along with their SD and IQR; t_E is also included. These statistics are tabulated analytically, as well as numerically, for the simple cases where the power D is 3, 2, 1, 1/2, and 1/3. Note how t_E, the median lifetime, and the IQR all lengthen as D decreases and the distribution of lifetimes $|\mathrm{d}f/\mathrm{d}t|$ widens. The mean lifetime diverges for $D \leqslant 1$, while the RMS and SD both diverge for $D \leqslant 2$. The values for $D = 2$ compare reasonably well with those above for the diffusion solution (10), if $t_0 \approx \bar{t}$.

For simple exponential decay (Eq. (5)), the median lifetime of the particles is identical to their half-life $t_{1/2} = t_0 \ln 2 \approx 0.6931 t_0$, their mean lifetime is just t_0, and their RMS lifetime is $\sqrt{2} t_0 \approx 1.4142 t_0$. In comparison, compressed exponential decay has a narrower distribution of lifetimes, while stretched exponential decay has a broader distribution. To illustrate, Table 10 lists the modal, median, mean, and RMS lifetimes for the Kohlrausch law (6), along with its SD and IQR; $t_E = t_0$ in all cases. These statistics are tabulated analytically, as well as numerically, for the particular cases $\beta = \infty$ and $\beta = 2$ (representing compressed exponential decay), $\beta = 1$ (corresponding to simple exponential decay), $\beta = 1/2$ and $\beta = 1/3$ (representing stretched exponential decay). Note that the lifetime distribution $|\mathrm{d}f/\mathrm{d}t|$ is a Dirac delta-function $\delta(t - t_0)$ for the extreme case $\beta = \infty$ of compressed exponential decay; as β decreases, the distribution of lifetimes widens, and its median, mean, and RMS spread farther apart, while its SD and IQR both increase.

References

Alvarellos, J.L., Zahnle, K.J., Dobrovolskis, A.R., Hamill, P., 2002. Orbital evolution of impact ejecta from Ganymede. Icarus 160, 108–123.

Alvarellos, J.L., Zahnle, K.J., Dobrovolskis, A.R., Hamill, P., 2005. Fates of satellite ejecta in the Saturn system. Icarus 178, 104–123.

Alvarellos, J.L., Zahnle, K.J., Dobrovolskis, A.R., Hamill, P., 2007. Transfer of mass from Io to Europa and beyond due to cometary impacts. Icarus, submitted for publication.

Armstrong, J.C., Wells, L.E., Gonzalez, G., 2002. Rummaging through Earth's attic for remains of ancient life. Icarus 160, 183–196.

Bellman, R.E., Kalaba, R.E., Lockett, J.A., 1966. Numerical Inversion of the Laplace Transform: Applications to Biology, Economics, Engineering, and Physics. Elsevier, New York.

Bevington, P.R., Robinson, D.K., 1969. Data Reduction and Error Analysis for the Physical Sciences, third ed. in 2003. McGraw–Hill, New York.

Burns, J.A., Gladman, B.J., 1998. Dynamically depleted zones for Cassini's safe passage beyond Saturn's rings. Planet. Space Sci. 46, 1401–1407.

Chambers, J.E., Quintana, E.V., Duncan, M.J., Lissauer, J.J., 2002. Symplectic integrator algorithms for modeling planetary accretion in binary star systems. Astron. J. 123, 2884–2894.

Dobrovolskis, A.R., Lissauer, J.J., 2004. The fate of ejecta from Hyperion. Icarus 169, 462–473.

Dobrovolskis, A.R., Alvarellos, J.L., Zahnle, K.J., 2000. A dynamical survey of the jovian system. Bull. Am. Astron. Soc. 32, 1116. Abstract.

Dones, L., Levison, H.F., Duncan, M., 1996. On the dynamical lifetimes of planet-crossing objects. In: Rettig, T.W., Hahn, J.M. (Eds.), Completing the Inventory of the Solar System. In: ASP Conference Series, vol. 107. Astron. Soc. Pacific, San Francisco, pp. 233–244.

Dones, L., Gladman, B., Melosh, H.J., Tonks, W.B., Levison, H.F., Duncan, M., 1999a. Dynamical lifetimes and final fates of small bodies: Orbit integrations vs Öpik calculations. Icarus 142, 509–524.

Dones, L., Levison, H.F., Zahnle, K., 1999b. Tossing out the leftovers: The fate of the remains of Earth's accretion. Bull. Am. Astron. Soc. 31, 1078–1079. Abstract.

Evans, N.W., Tabachnik, S., 1999. Possible long-lived asteroid belts in the inner Solar System. Nature 399, 41–43.

Farinella, P., Marzari, F., Matteoli, S., 1997. The disruption of Hyperion and the origin of Titan's atmosphere. Astron. J. 113, 2312–2316.

Frisch, U., 1995. Turbulence. Cambridge Univ. Press, UK.

Gladman, B., 1997. Destination: Earth. Martian meteorite delivery. Icarus 130, 228–246.

Gladman, B., Duncan, M., 1990. On the fates of minor bodies in the outer Solar System. Astron. J. 100, 1680–1693.

Gladman, B.J., Burns, J.A., Duncan, M.J., Levison, H.F., 1995. The dynamical evolution of lunar impact ejecta. Icarus 118, 302–321.

Gladman, B.J., Burns, J.A., Duncan, M., Lee, P., Levison, H.F., 1996. The exchange of impact ejecta between terrestrial planets. Science 271, 1387–1392.

Gladman, B., Michel, P., Froeschlé, C., 2000. The near-Earth object population. Icarus 146, 176–189.

Gladman, B., Dones, L., Levison, H.F., Burns, J.A., 2005. Impact seeding and re-seeding in the inner Solar System. Astrobiology 5, 483–496.

Halsey, T.C., Leibig, M., 1991. Stretched-exponential relaxation at a self-similar surface. Phys. Rev. A 43, 7087–7090.

Hartmann, W.K., 1972. Paleocratering of the Moon: Review of post-Apollo data. Astrophys. Space Sci. 17, 48–64.

Hartmann, W.K., Ryder, G., Dones, L., Grinspoon, D., 2000. The time-dependent intense bombardment of the primordial Earth–Moon system. In: Canup, R., Righter, K. (Eds.), Origin of the Earth and Moon. Univ. of Arizona Press, Tucson, pp. 493–512.

Holman, M.J., 1997. A possible long-lived belt of objects between Uranus and Neptune. Nature 387, 785–788.

Holman, M.J., Wisdom, J., 1993. Dynamical stability in the outer Solar System and the delivery of short period comets. Astron. J. 105, 1987–1999.

Lay, T., Wallace, T.C., 1995. Modern Global Seismology. Academic Press, San Diego.

Levison, H.F., Duncan, M.J., 1994. The long-term dynamical behavior of short-period comets. Icarus 108, 18–36.

Malyshkin, L., Tremaine, S., 1999. The Keplerian map for the planar three-body problem as a model for comet evolution. Icarus 141, 341–353.

Morbidelli, A., Froeschlé, C., 1996. On the relationship between Lyapunov times and macroscopic instability times. Celest. Mech. Dynam. Astron. 63, 227–239.

Nesvorný, D., Dones, L., 2002. How long-lived are the hypothetical trojan populations of Saturn, Uranus, and Neptune? Icarus 160, 271–288.

Nesvorný, D., Alvarellos, J.L.A., Dones, L., Levison, H.F., 2003. Orbital and collisional evolution of the irregular satellites. Astron. J. 126, 398–429.

Oberhettinger, F., Badii, L., 1973. Tables of Laplace Transforms. Springer-Verlag, New York.

Palmer, R.G., Stein, D.L., Abrahams, E., Anderson, P.W., 1984. Models of hierarchically constrained dynamics for glassy relaxation. Phys. Rev. Lett. 53, 958–961.

Peterson, I., 1989. Time to relax. Sci. News 135, 157–159.

Petit, J.-M., Hénon, M., 1987. A numerical simulation of planetary rings. II. Monte Carlo model. Astron. Astrophys. 188, 198–205.

Quintana, E.V., Lissauer, J.J., Chambers, J.E., Duncan, M.J., 2002. Terrestrial planet formation in the α Centauri system. Astrophys. J. 576, 982–996.

Robutel, P., Laskar, J., 2001. Frequency map and global dynamics in the Solar System. I. Short period dynamics of massless particles. Icarus 152, 4–28.

Rogers, S., 2005. Inverse Laplace transforms—A Matlab script. http://www/wolfson.cam.ac.uk/~ssr24/invlap.html.

Scher, H., Shlesinger, M.F., Bender, J.T., 1991. Time-scale invariance in transport and relaxation. Phys. Today 44, 26–34.

Shlesinger, M.F., Zaslavsky, G.M., Klafter, J., 1993. Strange kinetics. Nature 363, 31–37.

Tabachnik, S.A., Evans, N.W., 2000. Asteroids in the inner Solar System. I. Existence. Mon. Not. R. Astron. Soc. 319, 63–79.

Wetherill, G.W., 1977. Evolution of the Earth's planetesimal swarm subsequent to the formation of the Earth and Moon. Proc. Lunar Sci. Conf. 8, 1–16.

Wetherill, G.W., 1979. Steady state populations of Apollo–Amor objects. Icarus 37, 96–112.

Wikipedia, 2007. Stretched exponential function. http://en.wikipedia.org/wiki/Stretched_exponential_function.

Wisdom, J., Holman, M., 1991. Symplectic maps for the n-body problem. Astron. J. 102, 1122–1133.

Yabushita, S., 1980. On exact solutions of diffusion equation in cometary dynamics. Astron. Astrophys. 85, 77–79.

Zahnle, K., Alvarellos, J., Dobrovolskis, A., Hamill, P., 2007. Transfer of impact ejecta from Io to Europa. Lunar Planet. Sci. XXXVII. http://www.lpi.usra.edu/meetings/lpsc2007/pdf/2001.pdf.

Zeehandelaar, D.B., Hamilton, D.P., 2005. Material transport between the Galilean satellites. Bull. Am. Astron. Soc. 37, 762. Abstract.

Zeehandelaar, D.B., Hamilton, D.P., 2006. The fate of debris launched from the Galilean satellites. Bull. Am. Astron. Soc. 38, 674. Abstract.

Zeehandelaar, D.B., Hamilton, D.P., 2007. A local source for the Pioneer 10 and 11 circumjovian dust detections. In: Krüger, H., Graps, A. (Eds.), Dust in Planetary Systems. ESA Publication SP-643, pp. 103–106.